Theses and Dissertations   1. Thesis and Dissertation Collection, all items

1979

An adaptation and validation of a primitive variable mathematical model for predicting the flows in turbojet test calls and solid fuel ramjets

Stevenson, Charles Albert

Monterey, California : Naval Postgraduate School

https://hdl.handle.net/10945/18586

AN ADAPTATION AND VALIDATION
OF A PRIMITIVE VARIABLE MATHEMATICAL
MODEL FOR PREDICTING THE FLOWS
IN TURBOJET TEST CELLS AND
SOLID FUEL RAMJETS

Charles Albert Stevenson

NAVAL POSTGRADUATE SCHOOL
Monterey, California

THESIS

AN ADAPTATION AND VALIDATION
OF A PRIMITIVE VARIABLE MATHEMATICAL
MODEL FOR PREDICTING THE FLOWS
IN TURBOJET TEST CELLS AND
SOLID FUEL RAMJETS

by

Charles Albert Stevenson

June   1979

Thesis Advisor: D.W. Netzer

T195471

REPORT DOCUMENTATION PAGE		READ INSTRUCTIONS BEFORE COMPLETING FORM
1. REPORT NUMBER	2. GOVT ACCESSION NO.	3. RECIPIENT'S CATALOG NUMBER
4. TITLE (and Subtitle) An Adaptation and Validation of a Primitive Variable Mathematical Model for Predicting the Flows in Turbojet Test Cells and Solid Fuel Ramjets		5. TYPE OF REPORT & PERIOD COVERED Aeronautical Engineer's Thesis; June 1979
		6. PERFORMING ORG. REPORT NUMBER
7. AUTHOR(s) Charles Albert Stevenson		8. CONTRACT OR GRANT NUMBER(s) N6237679WR00014 N6053079WR30045
9. PERFORMING ORGANIZATION NAME AND ADDRESS Naval Postgraduate School Monterey, California 93940		10. PROGRAM ELEMENT, PROJECT, TASK AREA & WORK UNIT NUMBERS
11. CONTROLLING OFFICE NAME AND ADDRESS Naval Postgraduate School Monterey, California 93940		12. REPORT DATE June 1979
		13. NUMBER OF PAGES 74
14. MONITORING AGENCY NAME & ADDRESS(If different from Controlling Office)		15. SECURITY CLASS. (of this report) Unclassified
		15a. DECLASSIFICATION/DOWNGRADING SCHEDULE

16. DISTRIBUTION STATEMENT (of this Report)

Approved for public release; distribution unlimited.

17. DISTRIBUTION STATEMENT (of the abstract entered in Block 20, if different from Report)

18. SUPPLEMENTARY NOTES

19. KEY WORDS (Continue on reverse side if necessary and identify by block number)

Turbojet Test Cell
Solid Fuel Ramjet
Computer Flow Model

20. ABSTRACT (Continue on reverse side if necessary and identify by block number)

An adaptation of a primitive variable, finite-difference computer program was accomplished in order to predict the non-reacting flow fields in turbojet test cells and the reacting flow fields in solid fuel ramjets. The study compares the predictions of the primitive variable computer model with an earlier computer model and empirical data. It was found that the new model reasonably predicted the flow fields in both geometries. In

DD FORM 1 JAN 73 1473   EDITION OF 1 NOV 68 IS OBSOLETE
(Page 1)   S/N 0102-014-6601 |

(20. ABSTRACT Continued)

addition, the primitive variable model allowed simulation of test cell flows up to full engine throttle conditions and solid fuel ramjet flows which included an aft mixing chamber.

An Adaptation and Validation
of a Primitive Variable Mathematical
Model for Predicting the Flows
in Turbojet Test Cells and
Solid Fuel Ramjets

by

Charles Albert Stevenson
Lieutenant, United States Navy
B.S.E.E., University of Missouri, 1970

Submitted in partial fulfillment of the
requirements for the degrees of

MASTER OF SCIENCE IN AERONAUTICAL ENGINEERING

and

AERONAUTICAL ENGINEER

from the

NAVAL POSTGRADUATE SCHOOL
June 1979

ABSTRACT

An adaptation of a primitive variable, finite-difference computer program was accomplished in order to predict the non-reacting flow fields in turbojet test cells and the reacting flow fields in solid fuel ramjets. The study compares the predictions of the primitive variable computer model with an earlier computer model and empirical data. It was found that the new model reasonably predicted the flow fields in both geometries. In addition, the primitive variable model allowed simulation of test cell flows up to full engine throttle conditions and solid fuel ramjet flows which included an aft mixing chamber.

4

TABLE OF CONTENTS

LIST OF TABLES

6

LIST OF FIGURES

ABBREVIATIONS AND SYMBOLS

ROMAN SYMBOLS

A   Area

BP   Mass transfer (or "blowing") parameter

$\left.\begin{array}{l} C_1 \\ C_2 \\ C_D \end{array}\right\}$ $K-\varepsilon$ model empirical constants (Table I)

C_f Coefficient of friction

C_p Specific heat at constant pressure

E   9.0

g   Mass transfer conductance

G   Air mass flux

gr   Gram

h   Enthalpy

$\tilde{h}$ Stagnation enthalpy

H   Dimensionless enthalpy

h Heat transfer conductance

i   Stoichiometric coefficient

I   Turbulence intensity

K,k   Turbulence kinetic energy

$\tilde{K}$ Thermal conductivity

l   Length scale of turbulence

m   Mass fraction

M   Molecular weight

$\bar{M}$ Average molecular weight

$\dot{m}$ Mass flow

$\dot{m}''$ Mass flux

P,p	Pressure
$\dot{q}''$	Heat flux
r	Radial distance
R	Gas constant
$\overline{R}$	Universal gas constant
RR, $\dot{r}$	Regression rate
S	Source terms
St	Stanton number
T	Temperature
u	Axial velocity
v	Radial velocity
x	Axial distance
y_p^+	Dimensionless distance from solid boundary

GREEK SYMBOLS

Γ	Effective transport coefficient
δ	Incremental distance from wall
ΔH	Heat of combustion per Kg of fuel
ε	Turbulence dissipation rate
κ	von Karman constant
μ	Viscosity
ρ	Density
σ	Prandtl or Schmidt Number
τ	Shear stress
ϕ	Any variable
χ	$m_{fu} - m_{ox}/i$

SUBSCRIPTS

air	Air
atm	Atmosphere
bw	Fuel surface (or "blowing wall")
c	Conserved
eff	Effective
fg	Fuel grain
fp	Fuel port
fu	Fuel
in	Inlet
lam	Laminar
N2	Nitrogen
ox	Oxygen
p	Near wall node
pr	Products
ref	Reference
t	Turbulent
T	Total
w	Wall

ACKNOWLEDGMENT

Without the understanding, patience, encouragement
and guidance of my wife, Susan, and my Thesis Advisor,
Associate Professor David Netzer, this study would not have
been completed.

I.   INTRODUCTION

A.   BACKGROUND

During the past few years, there have been many advance-
ments in numerical techniques for predicting the behavior
of fluid flows. For example, several computer models have
been developed by Gosman, Spalding and others [1,2,3] which
use the mass, momentum and energy conservation equations
reduced to finite difference nonlinear algebraic form. The
development of reliable computer programs of this type
greatly benefits engineering analysis in such widely varying
fields as meteorology, aerodynamics and gasdynamics.

The earlier two-dimensional computer codes were based on
vorticity (ω) and stream function (ψ) [1,2,5]. This form
of the governing equations eliminates pressure and velocity
from immediate consideration. Pressure is normally calcu-
lated only after a converged solution is obtained. This
technique has several inherent disadvantages:

1. It results in large errors in the predicted pressure
distributions in all but quiescent flow regions due to the
higher order dependence of the pressure gradient on stream
function [6].

2. It is usually restricted to constant density flows
or to flows in which density varies only with temperature
[3,6].

3. The boundary conditions are difficult to specify
[3,4,5].

4. Considerable difficulty has been experienced in arriving at converged solutions, especially for non-uniformly spaced grids and high flow rates [2,5,6,7].

5. The $\psi-\omega$ model is not easily extended to three dimensional flows [3].

To overcome these difficulties, emphasis has been placed on developing computer codes based on velocity and pressure, the primitive variables.

A major problem with any new computer model is model validation. The difficulties of collecting accurate empirical data are multiplied when investigating three dimensional and/or reacting flows. In addition, many variables within these flows are not readily measurable (turbulence intensities, etc.).

An effort to utilize elliptic computer models which can handle turbulent, reacting, variable density flows at high subsonic and sonic velocities has been underway at the Naval Postgraduate School for several years. Two specific areas which have been investigated are flows in a turbojet test cell and in the combustion environment of a solid fuel ramjet.

B. TURBOJET TEST CELL

It is important to have the capability to test high performance jet engines throughout their operating envelope under conditions which approximate installed conditions. This is accomplished in blockhouse type installation called turbojet test cells (TJTC). The typical test cell incorporates

13

an inlet, a horizontal test section and a vertical exhaust
stack. The engine to be tested is normally mounted near
the center of the cell to allow the development of a nearly
uniform engine inlet velocity profile. The engine exhausts
into an augmentor tube which entrains additional air for
exhaust gas cooling and dilution. The quantity of this
secondary air is crucial to proper engine testing and test
cell performance. Each cell is equipped with adequate instru-
mentation to allow assessment of engine performance parameters.

Testing today's high power and high mass flow engines in
these installations produces a myriad of noise and air pollu-
tion problems. Cell modifications must often be made to
minimize these problems. This fact coupled with the future
need for larger, more expensive test cells to replace obso-
lete cells and to accommodate new generations of high tech-
nology engines, makes the development of reliable modeling
methods imperative. The frequently used one-dimensional models
are not adequate for predicting the details of the compli-
cated flows within a turbojet test cell and, therefore,
the cells often do not perform to their designed limits.
An accurate flow model would provide a needed design tool
which could help prevent costly design errors and improve
operating efficiency.

A two-dimensional $\psi-\omega$ computer code was used to analyze
the flows in a full scale and a subscale turbojet test cell
at the Naval Postgraduate School [2,6]. Experimental data
from the subscale test cell have been compared with

14

computations made with the computer model [6] and the latter has aided in design modifications and the evaluation of pollution control equipment on that installation. However, as discussed above, this analysis technique has several disadvantages.

A primitive variable (u-v-p) computer model could increase this prediction capability by extending it to specific geometries and flow rates that the ψ-ω model is incapable of predicting. In addition, a u-v-p model would more readily allow variable density flows to be analyzed and should more accurately predict augmentor pressure distribution.

C. SOLID FUEL RAMJET

A solid fuel ramjet (SFRJ) most often consists of a solid fuel grain which provides the walls for the combustion chamber [5]. Located at the air inlet end of the combustor is a sudden expansion or other type of flame stabilization device. The opposite end, downstream of the fuel grain, may also incorporate a sudden expansion aft mixing chamber. The primary combustion region is a turbulent diffusion flame which emanates from the forward recirculation zone and remains within the developing boundary layer. The aft mixing region may incorporate some means of injecting air for burning the fuel-rich mixture which has been found to exist there [5]. Mixing chamber and inlet design variables, fuel grain design and fuel properties make a wide variety of performance characteristics available.

The possibility of incorporating this type of propulsion device into future medium or long-range tactical weapon systems coupled with the expense of testing each new design, makes the development of a reliable computer model of this system highly desirable. The model could be used to predict the effects of fuel properties and to inexpensively evaluate different geometries and operating conditions. In addition, a three dimensional code would allow modeling discrete air injection into the aft mixing region. The latter technique can substantially increase combustion efficiency and allowable fuel loading.

Previous work at the Naval Postgraduate School has been directed toward improvement of the quantitative accuracy of the $\psi-\omega$ model and toward validation of that model [5]. Reasonable agreement with empirical data has been obtained. However, as previously stated, the $\psi-\omega$ model does not predict accurate pressure distributions and numerical difficulties prevented modeling the aft mixing chamber.

The purpose of this investigation was to adapt and validate a primitive variable, two-dimensional, finite difference computer code which models the flows within turbojet test cells and solid fuel ramjets.

II. MODEL OVERVIEW

A. INTRODUCTION

The computer model used in this study was adapted from the CHAMPION 2/E/FIX computer program developed by Pun and Spalding. As described in detail in reference 8, CHAMPION is a TWO-dimensional Elliptic, FIXed grid computer program which provides a solution of the conservation equations for recirculating flows in finite difference form.

B. ASSUMPTIONS

The flow was assumed to be steady, two-dimensional and subsonic. For simplicity the value of specific heat (C_p) was assumed to be constant although its dependence on temperature and/or composition could easily be included.

A modified Jones-Launder [8,10,11,12] two parameter turbulence model was incorporated to calculate the effective viscosity. It uses five empirical constants (Table I) and requires that two additional variables, turbulent kinetic energy (K) and turbulent dissipation rate (ε), be evaluated. Effective viscosity was calculated using the formulas:

$$\mu_{eff} = \mu_{lam} + \mu_t \qquad (1)$$

where

$$\mu_t = C_D \, \rho \, K^2 / \varepsilon \qquad (2)$$

17

For reacting flows, the four species, oxygen, nitrogen, fuel, and products, were considered. Simple, one-step, infinitely fast kinetics were assumed in which a fuel combines with an oxidant to form a single product without intermediaries [5,9].

1 gr fuel + i gr oxidizer → (1 + i) gr products
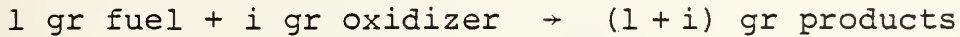
Fuel and oxygen, therefore, could not exist simultaneously and the combustion process was mixing limited. In addition, it was assumed that no oxygen existed at the fuel surface and that surface was isothermal. The turbulent Prandtl and Schmidt numbers were taken equal to unity and, therefore, the turbulent Lewis number was unity. The laminar Prandtl number was also taken to be unity.

C. GOVERNING EQUATIONS

The conservation equations for axi-symmetrical flows with no tangential variations can be put into the general form [8]:

$$\frac{\partial}{\partial x}(\rho u\phi) + \frac{1}{r}\frac{\partial}{\partial r}(\rho r v\phi) - \frac{\partial}{\partial x}(\Gamma_\phi\frac{\partial\phi}{\partial x}) - \frac{1}{r}\frac{\partial}{\partial r}(r\Gamma_\phi\frac{\partial\phi}{\partial r}) = S_\phi \quad (3)$$

convection terms   diffusion terms   source terms

where ϕ stands for the dependent variable $(u,v,k,\varepsilon,\tilde{h}$, etc.) being considered ($\phi = 1$ for the continuity equation), Γ_ϕ is the appropriate effective exchange coefficient for turbulent

18

flow and S_ϕ is the "source term" (Table II). The energy equation in terms of stagnation enthalpy has no source terms since the turbulent Prandtl and Schmidt numbers were chosen as unity and radiative transport was neglected [1,3]. Thus the stagnation enthalpy is given by:

$$\tilde{h} = h + (u^2 + v^2)/2 + K \qquad (4)$$

where for non-reacting flows:

$$h \equiv C_p T \qquad (5)$$

and for reacting flows:

$$h \equiv m_{ox} \Delta H/i + C_p(T - T_{ref}) \qquad (6)$$

The calculation of temperature was made using equations (4), (5) and (6). Density was calculated from the perfect gas law:

$$\rho = P/RT \qquad (7)$$

$$\begin{array}{l} \text{for non-reacting flows:} \quad R = \text{constant} \\ \text{for reacting flows:} \quad R = \overline{R}/\overline{M} \end{array} \qquad (8)$$

where,

$$1/\overline{M} = m_{fg}/M_{fg} + m_{ox}/M_{ox} + m_{N2}/M_{N2} + m_{pr}/M_{pr} \qquad (9)$$

For modeling reacting flows, two additional quantities, m_{N2} and $\chi \equiv m_{fu} - m_{ox}/i$, were evaluated. Each of these properties as well as stagnation enthalpy have identical governing differential equations (equation (3) with no source terms). In appropriate dimensionless form they also have identical boundary conditions. Thus, only one of the equations had to be solved. The dimensionless form selected for each property was:

$$H = (\tilde{h}_{in} - \tilde{h})/(\tilde{h}_{in} - \tilde{h}_{fg}) \qquad (10)$$

$$\overline{m}_{N2} = (m_{N2_{in}} - m_{N2})/(m_{N2_{in}} - m_{N2_{fg}}) \qquad (11)$$

$$\overline{\chi} = (\chi - \chi_{in})/(\chi_{fg} - \chi_{in}) \qquad (12)$$

In this study, stagnation enthalpy was calculated. H was then formed using equation (10). Since $H = \overline{m}_{N2} = \overline{\chi}$ at all points in the flow field, m_{N2} and χ could be calculated using equations (11) and (12). The mass fractions of fuel, oxygen, and products (m_{fu}, m_{ox}, m_{pr}) were found from the equations:

$$\text{for } \chi \geq 0; \quad m_{fu} = \chi, \quad m_{ox} = 0$$
$$(13)$$
$$\text{for } \chi < 0; \quad m_{fu} = 0, \quad m_{ox} = -\chi i$$

$$m_{pr} = 1 - m_{ox} - m_{fu} - m_{N2} \qquad (14)$$

20

D. CONSERVATION OF MASS

On each radial line the mass flow rate was calculated using the local density. The error in mass flow (compared to the summation of "mass-in" at all upstream boundaries) was used to uniformly adjust the axial velocity over the entire line. This process ensured that overall continuity was satisfied on the line. The pressure at all downstream locations was then adjusted to approximately correct for the momentum imbalance created by the uniform axial velocity adjustment. A "pressure correction" equation was then solved for each cell on the line. Local cell velocity (axial and radial) and pressure were then adjusted to satisfy cell-wise continuity. The details of this procedure are presented in reference 8.

E. BOUNDARY CONDITIONS

1. Introduction

Fixed boundary conditions were set at the desired or experimentally determined value and held constant. Specified gradient boundary conditions were handled by setting the appropriate convection/diffusion coefficient to zero in the finite difference equation ("breaking the link") and then entering the appropriate gradient through linearized "false" source terms [8]. The geometries and appropriate boundary conditions for the TJTC and SFRJ are summarized in figures 1 and 2.

21

2. Inlet

Although not a computer program limitation, "plug flow" was assumed at the inlets for both the SFRJ and TJTC. The secondary flow inlet of the TJTC was recessed approximately 0.3 meters (figure 1) to allow a velocity profile to develop over the length of the engine. Turbulent kinetic energy was selected to be uniform with a value which corresponded to the approximate turbulent intensity of the inlet flow.

3. Axis of Symmetry and Exit Plane

Radial and axial gradients were set equal to zero on the center line and exit respectively, with one exception; the radial flow velocity was zero.

4. Solid Boundaries

All non-reacting solid boundaries were considered adiabatic with both velocity components equal to zero ("no slip" condition).

For simplicity, a two part boundary layer was used. The border between the laminar sublayer and the turbulent layer was taken at $y_p^+ = 11.5$ [8]. y_p^+ was evaluated at each near wall node (p),

$$y_p^+ = (\rho \delta / \mu_{lam}) (\tau_w / \rho)^{1/2} \tag{15}$$

where, for $y_p^+ \geq 11.5$

$$\tau_w = C_D^{1/2} \rho K_p \tag{16}$$

22

τ_w was assumed uniform from the wall to the near wall grid point. Thus,

$$y_p^+ = C_D^{1/4} \, \rho \, K_p^{1/2} \, \delta / \mu_{lam} \qquad (17)$$

If $y_p^+ \geq 11.5$, the wall shear stress (τ_w) was calculated using the formula:

$$\tau_w = C_D^{1/2} \, \rho \, K_p = \rho \, C_D^{1/4} \, K_p^{1/2} (u/u^+)$$

$$= \kappa \, C_D^{1/4} \, \rho \, u_p \, K_p^{1/2} / \ln (E \rho \, \delta C_D^{1/4} K_p^{1/2} / \mu_{lam}) \qquad (18)$$

where

$$u^+ \equiv \frac{1}{\kappa} \ln (E \, y_p^+) \qquad (19)$$

Wall shear stress was evaluated for $y_p^+ < 11.5$ from the formula:

$$\tau_w = \mu_{lam} \, u_p / \delta \qquad (20)$$

Due to the steep gradients of properties in turbulent flows near solid boundaries, the source terms for K and ε at near wall nodes were expressed in terms of the wall shear stress [1,8]. τ_w also provides the boundary condition for the u and v equations. In the following equation for

turbulence dissipation rate (ε) at a near wall node (p),
the length scale is presumed proportional to the distance
from the wall (δ).

$$\varepsilon_p = C_D^{3/4} K_p^{3/2}/\kappa\delta \cong K_p^{3/2}/2.43\delta \qquad (21)$$

It was found, as was previously found by Netzer [5], that
when using the sudden expansion geometry in reacting flows
the near wall dissipation had to be increased on the step
face ($\varepsilon_p = K_p^{3/2}/0.4\delta$) and that the grid spacing adjacent
to the fuel surface had to be fine ($y_p^+ < 11.5$) in order
to obtain a temperature distribution in qualitative agree-
ment with experiment. Equation (20) implies that the wall
shear stress is calculated assuming a linear velocity pro-
file when $y_p^+ < 11.5$. A near-wall grid point, therefore,
can lie within the laminar sublayer, but the source terms
for K and ε imply that μ_{eff}/μ_{lam} is much greater than one
[10,11]. This fact precludes y_p^+ from being significantly
less than 11.5.

For reacting flows, the boundary conditions for the
dimensionless properties (equations (10), (11) and (12))
were zero at the inlet and unity "deep" in the fuel grain
(fg). These properties were considered to have zero gradients
on non-reacting surfaces.

The assumptions employed for reacting flows (unity
turbulent Prandtl and Schmidt numbers, simple chemical
reaction, constant specific heat and stagnation enthalpy

defined in equations (4) and (6)) result in a general boundary condition for all "conserved" properties (ϕ_c) [9] on a surface which has mass transfer,

$$\dot{m}_{bw}" = (\Gamma_\phi \frac{\partial \phi_c}{\partial r})_{bw} \Big/ (\phi_{c_{bw}} - \phi_{c_{fg}}) \tag{22}$$

where ϕ_c represents $\tilde{h}$, m_{N2} or $\chi \equiv m_{fu} - m_{ox}/i$.

A mass transfer conductance (g) is often defined such that,

$$(\Gamma_\phi \frac{\partial \phi_c}{\partial r})_{bw} = g(\phi_{c_\infty} - \phi_{c_{bw}}) \tag{23}$$

where ϕ_{c_∞} is defined as the free steam value. For this application, ϕ_{c_∞} was taken to be the local near wall value ϕ_{c_p}.

Substituting equation (23) into equation (22) yields:

$$\dot{m}_{bw}" = g(\phi_{c_p} - \phi_{c_{bw}})/(\phi_{c_{bw}} - \phi_{c_{fg}}) \tag{24}$$

$$\equiv g \, BP \tag{25}$$

where BP represents the mass transfer (or "blowing") parameter.

Without mass transfer the wall heat flux $(\dot{q}_w")$ can be defined in terms of the conditions at the near wall node.

$$\dot{q}_w" \;=\; \frac{h}{C_p}(h_w - h_p) \;=\; -\,(\frac{\tilde{K}}{C_p}\,\frac{\partial h}{\partial r})_w \tag{26}$$

where h_w is the enthalpy of the wall and h is the heat transfer conductance.

With $\phi_c = h$ in equation (23),

$$g \;=\; (\frac{\tilde{K}}{C_p}\,\frac{\partial h}{\partial r})_w \,/\,(h_p - h_w) \tag{27}$$

Substituting equation (26) into equation (27) yields:

$$g \;=\; h/C_p \tag{28}$$

or

$$g/(\rho u)_p \;=\; h/[(\rho u)_p\, C_p] \;\equiv\; St \tag{29}$$

thus,

$$g \;=\; (\rho u)_p\, St \tag{30}$$

From Reynold's Analogy with unity Prandtl number,

$$St \;=\; C_f/2 \;=\; \tau_w/(\rho u^2)_p \tag{31}$$

where C_f is the local friction coefficient.

Combining equations (30) and (31) yields:

$$g = \tau_w / u_p \tag{32}$$

Using the Couette flow approximation for the boundary layer behavior with mass transfer [9],

$$g = g^* \ln(1 + BP)/BP \tag{33}$$

where

$$g^* \equiv \lim_{BP \to 0}(g) \tag{34}$$

In this application, BP was evaluated from the solution of the energy equation using,

$$BP = (\tilde{h}_p - \tilde{h}_{bw})/(\tilde{h}_{bw} - \tilde{h}_{fg}) \tag{35}$$

The wall shear stress was calculated using equation (18) or equation (20) and modified with equation (33).

$$\tau_{bw} = \tau_w \ln(1 + BP)/BP \tag{36}$$

where τ_w is the wall shear stress without wall mass addition.

The mass transfer conductance (g) was found using equation (32). The wall mass flux was then evaluated using equation (25).

27

The wall heat flux ($\dot{q}_w$") on all solid isothermal boundaries was evaluated using Reynold's Analogy.

$$-\dot{q}_w"/(\tilde{h}_p - \tilde{h}_w) = \tau_w/u_p \tag{37}$$

$\dot{q}_w$" provides the boundary condition for the $\tilde{h}$ equation.

Since the blowing rates were small for the solid fuel ramjet (typically, BP < 2.0), K and ε were evaluated using equation (3) and the terms presented in Table II which incorporate the empirical constants of Table I.

Blowing velocity (v_{bw}) and fuel regression rate (RR) were calculated using the formulas:

$$v_{bw} = -\dot{m}_{bw}"/\rho_{bw} \tag{38}$$

$$RR = \dot{m}_{bw}"/\rho_{fg} \tag{39}$$

F. SOLUTION PROCEDURE

Five variables (u, v, K, ε and H or $\tilde{h}$) were solved using equation (3) in finite difference form. The line by line iterative procedure employed upwind differencing and under relaxation to promote convergence [8]. Pressure (relative to a selectable position and magnitude within the grid) was obtained from the mass conservation imposed on each radial grid line and on each nodal control volume as discussed above. Effective viscosity, temperature and density were also obtained as described above. A more detailed explanation of this procedure can be found in reference (8).

III.   RESULTS AND CONCLUSIONS

A.   TURBOJET TEST CELL

1.   Introduction

The purpose of this portion of the study was to utilize a primitive variable, finite difference computer program to analyze the flow within a turbojet test cell and to validate the model with data obtained from a subscale turbojet test cell located at the Naval Postgraduate School. Previous work [2,6,7] had accomplished this task for a $\psi-\omega$ computer model and, therefore, empirical data and the predictions of the $\psi-\omega$ model were available for comparison. The experimental data available consisted of augmentor wall pressure distributions and radial velocity profiles along the length of the augmentor tube for low, medium, and high engine flow rates.

As previously indicated, the $\psi-\omega$ model did a poor job of predicting pressure distributions in all but quiescent flow regions. Additionally, numerical convergence was difficult to obtain with that model when used to predict high velocity flows where compressibility effects are significant. It was anticipated that a primitive variable model would help to alleviate these difficulties. It is desirable to have a model which can be used to predict the flow field for full-throttle engine conditions where the engine exhaust flow is choked.

Adaptation of the primitive variable model to the subscale test cell geometry required the use of several approximations:

a. In modeling axi-symmetric flow, the engine was by necessity positioned at the axis of symmetry. In the actual test cell the engine was mounted closer to the deck than to the overhead. It would be expected, therefore, that the velocity distribution in the secondary flow (the flow around the engine) would be somewhat different than predicted.

b. The subscale test cell cross section is rectangular while the engine and augmentor tube are cylindrical. The system was modeled as three concentric cylinders with cross-sectional areas equivalent to the physical system. The nozzle exit area, the test section cross-sectional area and the empirical augmentation ratios and mass flow rates were used in calculating the axial inlet velocities used in both models.

c. The actual engine incorporated a converging nozzle. The engine was modeled as a cylinder with a diameter equal to the actual nozzle exhaust diameter.

d. In the model the augmentor inlet and the aft test cell wall were taken to be flush. The actual augmentor is often inserted into the test section which forms a recirculation zone above the augmentor tube. The effects on the augmentor flow field introduced by this recirculation region were shown to be minimal by Speakman, et al [7]. It should

be noted that the ψ-ω model incorporated this recirculation zone and a flow reducing lip flange on the augmentor inlet. When comparisons were made between the predictions of the two models, the effects of this recirculation zone and the augmentor inlet lip flange in the ψ-ω model were minimized by reducing their dimensions to one grid spacing.

Three of the flow conditions selected for model validation corresponded to conditions where empirical data were available. Model predictions for two additional conditions were made increasing the engine-to-augmentor inlet spacing to one and two engine diameters. No empirical data were available for the two latter conditions and, therefore, inlet parameters were simulated using empirical data for zero engine-to-augmentor entrance spacing. The test conditions are summarized in Table III.

Figures 3 through 7 compare predicted axial pressure distributions and radial velocity profiles obtained with the ψ-ω and u-v-p computer models. In addition, the available empirical data are also plotted on those figures. Pressure and velocity were selected for comparison because that was the extent of experimental data available. The velocity profiles from both computer models were plotted for the grid lines closest to the locations of the experimental data. In the cases where empirical data were not available, various representative velocity profiles were plotted for both models. Experimental pressure profiles were available only along the top of the augmentor tube. Predicted axial pressure

profiles are presented for various radial positions. These
locations are given as fractions of augmentor tube radius
(R_a). For example, the pressure distribution labeled
$R = 0.96\ R_a$ indicates that that distribution is along an
axial grid line located at a distance 96 percent of the aug-
mentor radius from the axis of symmetry. Two $\psi-\omega$ model axial
pressure profiles are depicted for each test condition. One
profile ($R = 0.38\ R_a$) lies in the quiescent flow region
between the engine and augmentor and was previously found
by Walters [6] to be the only location which produced a
reasonable estimate of the measured profiles. The second
axial pressure distribution ($R = 0.13\ R_a$) was located at
less than one engine radius of the center line. Three u-v-p
model axial pressure profiles are presented for each test
condition. One distribution ($R = 0.04\ R_a$) is near the axis
of symmetry. Another profile ($R = 0.28\ R_a$) runs along the
top of the engine and through the turbulent mixing region.
The third profile ($R = 0.96\ R_a$) is close to the augmentor
wall.

    2.   <u>Results and Discussion</u>

        a.   Test Case I - Low Flow Rate/Zero Spacing

            (1) Velocity Profiles

                As depicted in figure 3, both models pre-
dicted virtually identical velocity profiles at each station
along the augmentor tube. There was close agreement between
the predicted and the experimental velocity profiles at the
exit of the augmentor. The latter result was expected since

the velocity profile has become fully developed near the augmentor exit.

(2)   Pressure Profiles

(a) $\psi-\omega$ Model - This test condition had the lowest flow rates and offered the best chance for agreement with experiment. The initial pressure drop and the pressure rise are underpredicted in the outer flow region ($R = 0.38\ R_a$). Nearer the axis of symmetry ($R = 0.13\ R_a$) the initial pressure decrease is significantly overpredicted, but the magnitude (from minimum to maximum) and profile of the pressure rise were in good agreement with the experimental wall profile. The predicted pressure curves leveled off earlier than the experimental data. The difficulty in obtaining good pressure profiles with this model are evident. Near the augmentor exit there should be negligible radial pressure variations. The solution was converged in all dependent variables (Table IV) and negligible pressure variation was calculated in the radial direction near the augmentor exit. However, the pressure profiles along the two axial locations presented did not become equal near the augmentor exit. The latter resulted from the large errors in the predicted profiles near the augmentor inlet.

(b)   u-v-p Model - All three u-v-p profiles predicted an initial pressure drop above the engine which was not indicated experimentally. Both the pressure drop and rise within the augmentor were underpredicted. However, the primitive variable model more accurately predicted

33

the location of the minimum pressure and seemed to level

off at approximately the same augmentor position as the

experimental data. Walters and Netzer [6] have previously

shown that the model predicts that mixing is nearly complete

at the location where the pressure profile levels off and

that, simultaneously, the velocity distribution approaches

a fully developed profile. Experimental data confirmed this

characteristic. Figure 3 indicates that, as anticipated,

the u-v-p model can more accurately predict the location

at which turbulent mixing is complete. It also predicted

very little pressure variation with radial augmentor posi-

tion as is known to be true experimentally.

      b.   Test Case IIA - Medium Flow Rate/Zero Spacing

         (1) Velocity Profiles

         The results are presented in figure 4 and,

again, both computer predictions were very similar and

agreed with the limited experimental data at the augmentor

exit plane.

         (2) Pressure Profiles

         (a) ψ-ω Model - The pressure profile

nearest the center line became more unrealistic for this

higher flow rate condition. The initial pressure drop was

greatly exaggerated; however, the magnitude of the pressure

rise was again in good agreement with experiment. The pres-

sure profile in the quiescent flow region ($R = 0.38\ R_a$) did

not agree with the experimental curve. A premature pressure

drop was predicted and this model underestimated both the

pressure drop and rise in the augmentor tube. In addition, the minimum pressure point was predicted to occur about one engine diameter downstream of the experimental minimum.

(b) u-v-p Model - As for Case I, the u-v-p model predicted a small pressure drop above the engine which was not indicated by the experimental measurements. It also consistently underpredicted the augmentor pressure drop and rise. The slope of the pressure rise, however, was in reasonable agreement with experiment.

c. Test Case IIB - Medium Flow Rate/One Engine Diameter Spacing

(1) Velocity Profiles

Experimental data were not available for this test condition. The predicted profile are presented in figure 5 and show that the two computer models predicted velocity profiles which were in close agreement. The primitive variable model, however, predicted a slightly greater initial jet spreading at the augmentor entrance and required a slightly longer duct length to obtain a fully developed profile.

(2) Pressure Profiles

(a) ψ-ω Model - As for Case IIA, the centermost pressure distribution greatly exaggerated the initial pressure drop. In this case, the pressure rise also appeared to be much too rapid in comparison to the $R = 0.38\ R_a$ profile and the u-v-p profiles. The profile in the quiescent flow region was in reasonable agreement with the wall profile

35

obtained with the u-v-p model. The slopes of the pressure
rise and the minimum pressure predicted by both models were
nearly identical. The ψ-ω model, however, again predicted
the minimum pressure to occur somewhat farther downstream
than did the u-v-p model.

         (b) u-v-p Model - For this case, the
pressure profile closest to the augmentor wall had a signi-
ficantly lower minimum pressure than the other profiles.

     d.   Test Case IIC - Medium Flow Rate/Two Engine
         Diameter Spacing

      (1)   Velocity Profiles

         No empirical data were available for this
test condition. The computer predictions are presented in
figure 6. As for Case IIB, the primitive variable model
predicted greater initial jet spreading. In this case,
however, the ψ-ω velocity profiles became flat and the
pressure profiles leveled off considerably upstream of the
u-v-p predicted profiles.

      (2)   Pressure Profiles

         (a)   ψ-ω Model - The centermost pressure
profile was completely unrealistic. The quiescent region
profile indicated a larger pressure drop and rise and a
minimum pressure point farther downstream than the other
model. In addition, the ψ-ω model profile leveled off much
earlier.

         (b) u-v-p Model - Again the minimum pressure
was obtained for the profile closest to the augmentor wall

and was located just inside the augmentor entrance. All
the primitive variable curves indicate a more gentle aug-
mentor pressure rise, leveling about midway down the augmentor
tube.

        e.   Test Case III - High Flow Rate/Zero Spacing

           (1)   Velocity Profile

                As indicated in figure 7, substantially more
experimental data were available for this test condition.
In the experiment the nozzle was operated with a pressure
ratio (p_{atm}/P_T) less than critical for one dimensional isen-
tropic flow. However, using the experimental nozzle flow
rate and approximating the nozzle flow as one-dimensional and
isentropic resulted in a nozzle exit Mach number of approxi-
mately 0.95. This condition was imposed on the models. As
has been observed for the previous test cases, the velocity
profiles for both models are quite similar and in reasonably
good agreement with experiment. However, the predicted pro-
files for both models tended to flatten a little too rapidly.
The primitive variable model again predicted slightly more
initial jet spreading at the augmentor inlet and less mixing
down the augmentor tube than did the $\psi-\omega$ model. The experi-
mental data more nearly agreed with the $\psi-\omega$ model at the
augmentor inlet and with the u-v-p model downstream.

           (2)   Pressure Profiles

              (a) $\psi-\omega$ Model - Again the center pressure
profile was completely unrealistic. The quiescent region
pressure profile predicted the augmentor pressure drop to

begin prior to the engine exit, and underpredicted the augmentor pressure drop and rise. The minimum pressure position was substantially displaced down the augmentor tube and the slope of the pressure rise did not agree with experiment.

(b) u-v-p Model - Aside from the unexplainable pressure spike at the augmentor inlet for the centerline pressure profile, all three u-v-p pressure profiles were quite similar. They underpredicted both the augmentor pressure drop and rise. The slope of the pressure rise was in good agreement with experimental data within the first half of the augmentor tube. Both the $\psi-\omega$ and u-v-p models' predicted pressure profiles leveled off before the experimental curves.

3. Comparison of Computational Accuracy and Required Computer Time

The utility of any computer program using numerical methods is reflected by the amount of CPU time required and the ease of arriving at converged solutions. Table IV compares the percentage change in variable magnitude on successive iterations and the required CPU time.

A considerable savings in CPU time was obtained using the line-by-line iterative procedure of the primitive variable model in lieu of the point-by-point (Gauss-Seidel) method employed in the $\psi-\omega$ model.

At low flow rates, the convergence was quite similar for both models. However, at higher flow rates the u-v-p model had better convergence in less time.

38

4. <u>Computer Related Problems</u>

Both models required that the proper relaxation parameters be selected in order to obtain convergence. The lack of any procedure for selecting the proper relaxation values makes this process quite time consuming. Previous research using the ψ-ω model facilitated the selection of these parameters for that model. It was found that the u-v-p model was quite sensitive to the calculated "pressure corrections". Obtaining the correct underrelaxation value for pressure proved to be the key in arriving at a converged solution for the primitive variable model.

The line-by-line iterative procedure used in the u-v-p model was, as expected, quite good in propagating disturbances downstream when iterating from left to right. A downstream disturbance is propagated upstream by successive iterations through the entire field. This fact, at least for a geometry incorporating a sudden contraction, made the convergence dependent on the number of traverses on each radial line. An excessive number of traverses would cause divergence. The number of traverses on each line was con-trolled in two ways. After each traverse, residual factors were calculated for each variable and the largest residual factor was compared to a preset value. If the largest residual was less than the preset value, the program advanced to the next radial line. The program would also advance when a preset maximum number of traverses had been completed on any radial line. To aid convergence, the program was

held to a few traverses on each line until several field iterations had allowed the presence of the contraction wall to be "felt" upstream. The number of traverses on a line was then increased. It was additionally found that when working with coaxial flows with radically different inlet velocities, the normalizing factors (which were based on average inlet conditions and used to calculate the residual values on each line) resulted in excessive traverses being made in regions of high flow velocity. Repeated calculations on radial lines which had already converged often caused divergence. Adjusting the normalizing factors downstream of the engine exit alleviated this problem.

The primitive variable model demonstrated some convergence difficulty in the recirculation region adjacent to the sudden contraction. This problem could have resulted from the relatively large normalizing factors used in this local region of low velocity or, as suggested by Launder and Spalding [12], it could have possibly been due to the inadequacy of the empirical constants (Table I) in the K-ε model to adequately describe the flow in this quiescent zone.

As with any finite difference numerical solution, grid spacing was found to be critical. To aid convergence, the grid spacing approaching any solid boundary was decreased and grid lines were packed into regions of large property gradients. Care must be exercised in picking successive grid sizes. Gosman, et al [1] recommended that for the $\psi - \omega$ model successive spacing should not increase by more

than about a factor of 1.5. This restriction was also
employed for the primitive variable model. In simulating
the TJTC, a 30 by 30 grid system was utilized for the primitive
variable model. A 43 by 40 grid was required for the ψ-ω
model.

5. Summary of Results

In most cases the predicted velocity profiles for
both the ψ-ω and u-v-p computer models agreed with each
other and with the available experimental data. The u-v-p
model predicted more initial jet spreading at the augmentor
inlet, especially in those cases where the engine exit
plane was not flush with augmentor inlet. Both models pre-
dicted that a flat velocity profile was obtained where the
pressure profile leveled off. For the one case in which
experimental data were available over the entire length of
the augmentor tube, the predicted velocity profiles seemed
to flatten slightly faster than the experimental data.

In general, the ψ-ω model demonstrated poor pressure
prediction capability. For low flow rates the pressure rise
on the wall from minimum to maximum was accurately predicted
for a pressure profile calculated near the axis of symmetry.
For higher flow rates the centermost predictions became
unrealistic although converged solutions were obtained for
all primary variables. For the predicted pressure profiles
along axial lines that were in the quiescent flow region, the
ψ-ω model characteristically underpredicted the pressure
drop and rise along the augmentor wall. The minimum predicted

41

pressure location was typically somewhat downstream of its experimentally determined position. In addition, contrary to experimental evidence, the ψ-ω model predicted the start of the pressure decrease significantly upstream of the engine exit plane.

The primitive variable model showed little radial pressure variation with radial augmentor position except near the engine exit plane. It consistently predicted an erroneous but small pressure drop above the engine. It seemed to accurately locate the minimum pressure position and to predict the rapid pressure drop at the augmentor entrance. It consistently underpredicted the pressure drop and rise in the augmentor but tended to accurately predict the slopes of the rising pressure profiles. Application of the K-ε turbulence model with fixed parameters (C_D, C_1, C_2, σ_ε, σ_K) to the test cell flow conditions may be the major reason for the lack of quantitative accuracy in the predicted pressure profiles. Further experimental data (for example, turbulence intensity measurements) are needed to determine the models applicability to the low velocity region surrounding the engine. As indicated in figures 3 through 7, there were some significant differences between experimental and predicted "pressure differentials" at the augmentor exit. Calculations indicate, however, a maximum of two percent error in absolute pressure at that location. Therefore, continuity was satisfied within acceptable limits using the virtually identical predicted and experimental velocity profiles.

The primitive variable model appears to reasonably predict the TJTC flow field up to sonic engine exhaust conditions. These predictions include realistic pressure distributions and require substantially less computer time and fewer grid lines than the $\psi-\omega$ model.

B. SOLID FUEL RAMJET

1. Introduction

The purpose of this portion of the study was to use a primitive variable, finite-difference computer program to determine the flow within a solid fuel ramjet combustor with emphasis on the aft mixing chamber. The model was then used to investigate the effects of air flow rate through the fuel port on the combustion in the aft mixing chamber. As previously explained, an aft mixing region allows further combustion aft of the fuel grain. This process increases combustion efficiency. Lowering the inlet flow rate increases the fuel-air ratio within the combustion region. Bypass air can then be injected into the aft mixing region. The latter procedure can be used to appreciably increase fuel loading. Previous work at the Naval Postgraduate School [5,13,14] modeled a SFRJ with a computer program utilizing $\psi-\omega$ as primary variables. Numerical instabilities, however, prevented the use of the $\psi-\omega$ model to predict the flow in the aft mixing region. The results of that investigation and some empirical data were available for comparison with the predictions from the primitive variable model.

43

Several factors were anticipated which could contribute to differences in the predictions of the two models and the empirical data:

a. Some of the experimental data were measured in cold, non-reacting flows.

b. The incorporation of the aft mixing chamber into the primitive variable model could influence the flow upstream in the combustion chamber.

c. In the $\psi-\omega$ model, a wall value of turbulent kinetic energy (K) was specified through a slip factor such that K_w = -1.0 or -0.39*K_p, depending on the magnitude of the turbulent Reynold's number. In the u-v-p model the boundary condition for K at the near wall node (p) was specified in terms of the wall shear stress. In addition, in the primitive variable model, the boundary condition for stagnation enthalpy at the near wall node was made a function of wall shear stress through Reynold's Analogy. These factors affect heat flux to the wall and, therefore, the fuel regression rate.

d. The u-v-p model used a 23 by 21 grid in the fuel chamber while the $\psi-\omega$ model used a 17 by 25 grid. In reality the heat of vaporization of the fuel is a fixed quantity and, if converged solutions are obtained, the wall heat flux should not depend upon the grid spacing. However, it has been found [5] that the heat flux to the wall (which is calculated using the near-wall grid point) is a function of

44

the grid distance from the wall. This results from the assumed behavior of the variables near the wall. The procedure employed in this study was to adjust the heat of vaporization to match the empirical fuel regression rate at one air flow rate and to use that value for all other flow rates. If the model is realistic, fuel regression rate should then vary with air flow rate in agreement with experiment.

2. Results and Discussion

a. Regression Rate

Figure 8 shows that the fuel regression rate predictions of the u-v-p and $\psi-\omega$ models are quite similar. Both predict the peak regression rate upstream of experiment and have similar slopes. This early peak in the regression rate results from the model predicting a shorter reattachment length than was found experimentally [5]. The primitive variable model predicted a higher regression rate but, as previously discussed, the magnitude can easily be adjusted through the value used for the heat of vaporization of the fuel.

Figure 9 shows the effects of increasing inlet air mass flux ($G = \dot{m}_{air}/A_{fp} \propto V_{in}$) on fuel regression rate ($\dot{r}_{fu}$). The regression profile remained the same and, as expected, decreased with decreasing G. It has been found experimentally [13] that fuel regression rate varies as the air mass flux raised to a constant power ($\dot{r}_{fu} \propto G^n$). Boaz and Netzer [13] found that this constant was equal to 0.41

while Mady, et al [14] found it to be approximately 0.38. For the three test cases of this study, the u-v-p model predicted the constant, n, to be between 0.31 and 0.34. Thus, the primitive variable model appears to correctly predict the nature of the change in convective heat flux to the fuel surface with air flow rate.

b. Turbulence Intensity

Figure 10 compares the predicted centerline turbulence intensity (assuming isotropic turbulence) and experimental data for non-reacting flow. The primitive variable computer model slightly underpredicted the peak turbulence intensity while the ψ-ω model overpredicted it. Both models predicted the peak occurring downstream of experiment and both distributions seem to be approaching an identical asymptote downstream. The decrease in turbulence intensity predicted by the ψ-ω model near the inlet resulted from the model over-predicting the velocity increase as the air entered the combustor [5]. The u-v-p model overcame this difficulty. The differences in the results from the two computer models may result from the differences in the boundary conditions on turbulent kinetic energy in the combustor and/or to the effects of the addition of the aft mixing chamber on the upstream flow. Both of these phenomena have already been discussed. It should also be noted that the experimental data used in this comparison was measured in a non-reacting flow.

Figure 11 shows the effect of decreasing inlet air mass flux on turbulence intensity. As anticipated, the peak turbulence intensity decreased as inlet axial velocity decreased. Each test condition, however, converged on the same value downstream. Much additional experimental work is required to obtain the turbulence intensities in reacting flows; only then can the adequacy of the K-ε turbulence model be fully evaluted.

    c. Pressure

Figure 12 shows the effect of inlet velocity on the axial pressure distributions for the three primitive variable test conditions (Table V). (The radial scale has been expanded to illustrate the pressure variations. The maximum pressure variation is approximately 1.2 psi.) Like the predicted pressure profiles of the TJTC, the radial location of these distributions are given as a fraction of the fuel port radius (R_{fp}). As expected, pressure initially increased due to jet spreading. This was followed by a slight pressure drop as the flow accelerated due to heat addition and wall friction. The final pressure rise was due to jet spreading in the aft mixing region.

    d. Temperature

Figure 13 displays radial temperature variations in the combustor near the end of the fuel grain and at about 1.5 aft mixing region diameters down the aft chamber. As discussed above, fuel flow rate decreases less than inlet air flow rate ($\dot{r}_{fu} \propto G^n$, $n < 1$). Therefore, as air flow rate

47

is decreased, the overall mixture ratio becomes more fuel
rich, and the developing boundary layer and the fuel layer
between the diffusion flame and the wall thickens. Thus,
as shown in figure 13, as the inlet velocity (and, therefore,
the inlet air mass flux) was decreased, the maximum tempera-
ture (or "flame") in the combustor moved away from the fuel
grain and the centerline temperature increased. The maximum
temperature in the aft mixing chamber was also predicted
to occur farther from the top wall.

   Figure 14 shows similar data predicted by the
ψ-ω model slightly farther upstream. A significant differ-
ence between the predictions of the two computer models was
that the ψ-ω model predicted a stronger dependence of the
peak temperature radial location on the inlet air velocity.
An aft mixing region was not incorporated into the ψ-ω model.
Therefore, the boundary layer continued to grow and the point
of maximum temperature continued to recede from the fuel sur-
face with increasing axial distance from the initial reattach-
ment point. The aft mixing region of the u-v-p model caused
the boundary layer thickness (and, therefore, the location
of the peak temperature) to become approximately constant
in the latter portion of the combustion chamber. This was
the apparent cause of the weaker dependence predicted by
the u-v-p model of peak temperature location and boundary
layer thickness on inlet air mass flux.

e. Aft Mixing Region

Figure 15 is an illustration of the predicted combustion behavior in the aft mixing region. (The radial dimension has been expanded for clarity.) Lines of maximum temperature (i.e., the flame sheet location) are presented as a function of fuel grain inlet air velocity. It should be noted that the aft recirculation zone, which is also depicted on this figure, was predicted to be fuel rich and did not vary appreciably in size with changing inlet air mass flux. As discussed above, the fuel regression rate decreased more slowly than inlet air flow rate. Thus, as air flux was decreased the mixture entering the aft chamber became more fuel rich and the thickness of the fuel layer at the end of the fuel grain increased slightly. With high air mass flux the flame reached the wall, resulting in complete combustion. This condition could be expected to produce a high combustion efficiency. For the lower air flow rates, the flame did not reach the wall. This would result in unburned fuel entering the nozzle and a lower combustion efficiency. This effect can also be seen in figure 13. As the inlet axial velocity was decreased, the maximum temperature region ("flame zone") progressively moved farther from the wall. These predictions might be used as a first approximation for predicting the "best" placement of bypass air dumps in the aft mixing region. To predict an optimum location, however, the primitive variable model would have to be expanded to three dimensions.

3. Computer Related Problems

As has been discussed previously, in order to obtain
results that were in agreement with experiment, the grid
spacing near the fuel surface was required to be fine and
the length scale of turbulence was decreased on the combustor
step face. Because convergence was sensitive to the length-
to-width ratio of individual control volumes, the small
radial grid spacing near the fuel surface forced similar
fine spacing in the axial direction downstream in the aft
mixing region. A length to width ratio of less than ten to
one was required. These criteria forced the use of a large
number of cells, which in turn required a large amount of
CPU time. A typical primitive variable 40 by 33 grid required
75 to 80 minutes of CPU time to converge. A typical $\psi-\omega$
model with a 17 by 25 grid required 35 to 40 minutes of CPU
time. It must be remembered, however, that numerical
instabilities prohibited the modeling of an aft mixing
chamber with the $\psi-\omega$ model.

The primitive variable model demonstrated some con-
vergence difficulty in the aft recirculation region. This
problem seemed to be associated with the continually changing
velocity profile just prior to the aft expansion (the "inlet"
conditions for the aft mixing chamber). This effect was
suppressed by iterating through the entire flow field several
times with only a few traverses on each line and then increas-
ing the number of traverses on the radial grid lines in the
aft mixing region once the combustor flow field had essentially
converged.

4. Summary of Results

In general, the predicted flow fields for the two computer models were quite similar within the combustor. As anticipated, the primitive variable model allowed the prediction of the flow within the aft mixing region. This was not possible with the $\psi-\omega$ model. The presence of the aft mixing region coupled with the few boundary condition differences previously mentioned, had some effect on the flow field predictions in the ramjet combustion chamber. The most noticeable of these were the decrease in dependence of the boundary layer thickness and the maximum temperature radial location on axial inlet velocity. Many additional empirical data are needed to completely assess the validity of the primitive variable model in predicting the flow in a SFRJ. The primitive variable model, however, reasonably predicted the solid fuel ramjet flow field and enabled the simulation of an aft mixing region.

C_1	C_2	C_D	$\sigma_{k,eff}$	$\sigma_{\varepsilon,eff}$
1.43	1.92	0.09	1.0	1.3

TABLE I.   K-ε TURBULENCE MODEL EMPIRICAL CONSTANTS

ϕ	Γ_ϕ	S_ϕ
u	μ_{eff}	$-\dfrac{\partial P}{\partial x} - \dfrac{2}{3}\dfrac{\partial}{\partial x}\{\dfrac{\mu}{r}[\dfrac{\partial}{\partial x}(ru) + \dfrac{\partial}{\partial r}(rv)]\} + \dfrac{\partial}{\partial x}(\mu \dfrac{\partial u}{\partial x}) + \dfrac{1}{r}\dfrac{\partial}{\partial r}(\mu r \dfrac{\partial v}{\partial x})$
$\bar{v}$	μ_{eff}	$-\dfrac{\partial P}{\partial r} - 2\dfrac{\mu v}{r^2} - \dfrac{2}{3}\dfrac{\partial}{\partial r}\{\dfrac{\mu}{r}[\dfrac{\partial}{\partial x}(ru) + \dfrac{\partial}{\partial r}(rv)]\} + \dfrac{\partial}{\partial x}(\mu \dfrac{\partial u}{\partial r}) + \dfrac{1}{r}\dfrac{\partial}{\partial r}(\mu r \dfrac{\partial v}{\partial r})$
TKE	μ_{eff}/σ_k	$\mu_t\{2[(\dfrac{\partial u}{\partial x})^2 + (\dfrac{\partial v}{\partial r})^2 + (\dfrac{v}{r})^2] + (\dfrac{\partial u}{\partial r} + \dfrac{\partial v}{\partial x})^2\} - \rho\varepsilon$
TED	$\mu_{eff}/\sigma_\varepsilon$	$\dfrac{C_1\varepsilon}{k}\{\mu_t(2[(\dfrac{\partial u}{\partial x})^2 + (\dfrac{\partial v}{\partial r})^2 + (\dfrac{v}{r})^2] + (\dfrac{\partial u}{\partial r} + \dfrac{\partial v}{\partial x})^2)\} - \dfrac{C_2\rho\varepsilon^2}{k}$
$\tilde{h}$	μ_{eff}/σ_h	0
$\dfrac{m_{ox}}{i} - m_{fu}$	μ_{eff}/σ_j	0
m_{N2}	μ_{eff}/σ_j	0

$\sigma_j = \sigma_k = \sigma_h = 1 \;,\; \sigma_\varepsilon = 1.3$

$C_1 = 1.45 \quad C_2 = 2.0 \quad v_\theta = 0$

TABLE II. GOVERNING EQUATION PARAMETERS

CASE	$\dot{m}_e$ [kg/sec]	A.R.	Spacing [M]	P_{in}^* [N/M^{2}x10^{-5}]	P_e^{**} [N/M^{2}x10^{-5}]	T_{in}^* [°K]	T_e^{**} [°K]	u_e^{**} [m/sec]
I	0.45	2.26	0	1.013	1.013	288.9	287.8	187.8
IIA	0.69	3.12	0	1.010	1.010	289.4	270.0	272.5
IIB	0.69	3.12	0.05	1.010	1.010	289.4	270.0	272.5
IIC	0.69	3.12	0.10	1.010	1.010	289.4	270.0	272.5
III	0.99	2.89	0	1.009	1.242	289.4	263.9	310.0

*Test cell at engine inlet

**Nozzle exhaust

TABLE III. TUBROJET TEST CELL TEST CONDITIONS

54

TABLE IV. COMPARISIONS OF CPU TIME AND $(\Delta\phi/\phi)\cdot 100$ FOR LAST CALCULATION

	CPU TIME (MIN)	VORTICITY	STREAM FUNCTION	AXIAL VELOCITY	PRESSURE MINUS REF PRESSURE	TURBULENT KINETIC ENERGY	DISSIPATION RATE
CASE I mass flow = .45 kg/sec AR = 3.26 spacing = 0	138.5 / 21.6	.15 / –	.041 / –	– / 1.17 / 0	– / .24 / 0	.19 / .11 / 0	.0004 / .15 / .15
CASE IIA mass flow = .69 kg/sec AR = 3.12 spacing = 0	139.2 / 29.1	.20 / –	.08 / –	– / .64 / .12	– / .68 / .68	.27 / .36 / .36	.003 / .03 / 0
CASE IIB mass flow = .69 kg/sec AR = 3.12 spacing=1 eng dia	145.4 / 32.9	.79 / –	.18 / –	– / 0 / .12	– / .28 / 0	.32 / 0 / 0	.0003 / 0 / 0
CASE IIC mass flow = .69 kg/sec AR = 3.12 spacing=2 eng dia	159.3 / 20.8	3.1 / –	.44 / –	– / 0 / 0	– / .63 / .63	3.14 / .46 / 0	3.5 / .16 / .16
CASE III mass flow = .99 kg/sec AR = 2.9 spacing = 0	148.7 / 22.8	.43 / –	.098 / –	– / .55 / 0	– / .15 / .15	.29 / .07 / 0	.001 / .08 / 0

Legend:
— $\psi - \omega$ model - worst case in field
— U-V-P model - worst case in augmentor
— U-V-P model - worst case in field

CASE	$r_{in}(m)$	$\dot{m}_{air}(kg/sec)$	u_{in} (m/sec)	G (kg/m^2-sec)
1	.00681	.08049	197.0	70.6
2	.00681	.07274	178.0	63.8
3	.00681	.06442	157.6	56.5

TABLE V. SOLID FUEL RAMJET TEST CONDITIONS
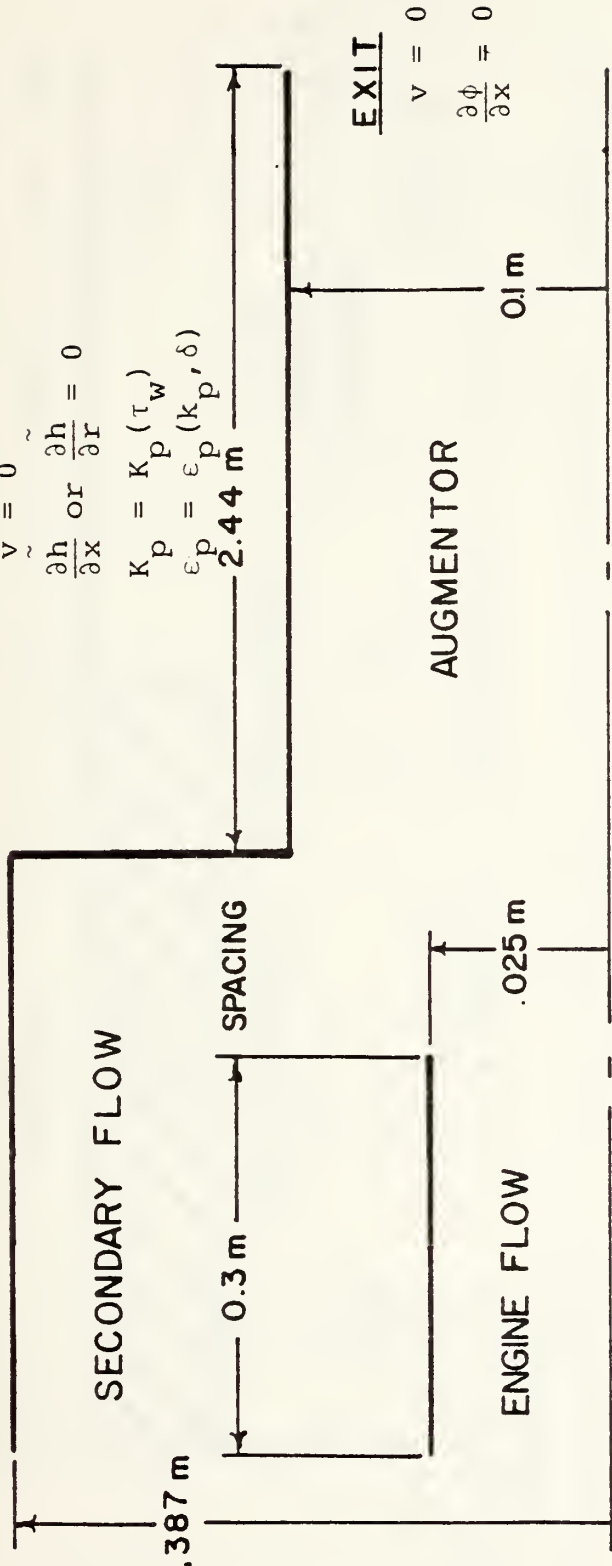
FIGURE 1. TURBOJET TEST CELL GEOMETRY AND BOUNDARY CONDITIONS

EXIT

$v = 0$

$\dfrac{\partial \phi}{\partial x} = 0$

NON REACTING WALLS

$u = 0$

$v = 0$

$\dfrac{\partial \phi_c}{\partial x}$ or $\dfrac{\partial \phi_c}{\partial r} = 0$

$k_p = k_p(\tau_w)$

$\varepsilon_p = \varepsilon_p(k_p, \delta)$

AFT MIXING CHAMBER

.158 m

.027 m

IN FUEL GRAIN

$u = 0$

$v = 0$

$\tilde{h} = -h_{fg}$

$\phi_c = 1$

non-dimensional

CENTER LINE

$v = 0$

$\dfrac{\partial \phi}{\partial r} = 0$

FUEL

.3048 m

FUEL SURFACE

$u = 0$

$v = v_{bw}$

$\tilde{h} = 0$

$k_p = k_p(\tau_w, BP)$

$\varepsilon_p = \varepsilon_p(k_p, \delta)$

INLET

$u = u_{in}$

$v = 0$

$k = .005 \cdot u_{in}^2$

$\varepsilon = .09 k^{3/2} / .03 r$

$\chi = -m_{ox_{in}} / i$

$\phi_c = 0$

non-dimensional

.019 m

AIR INLET

.006 m AIR INLET
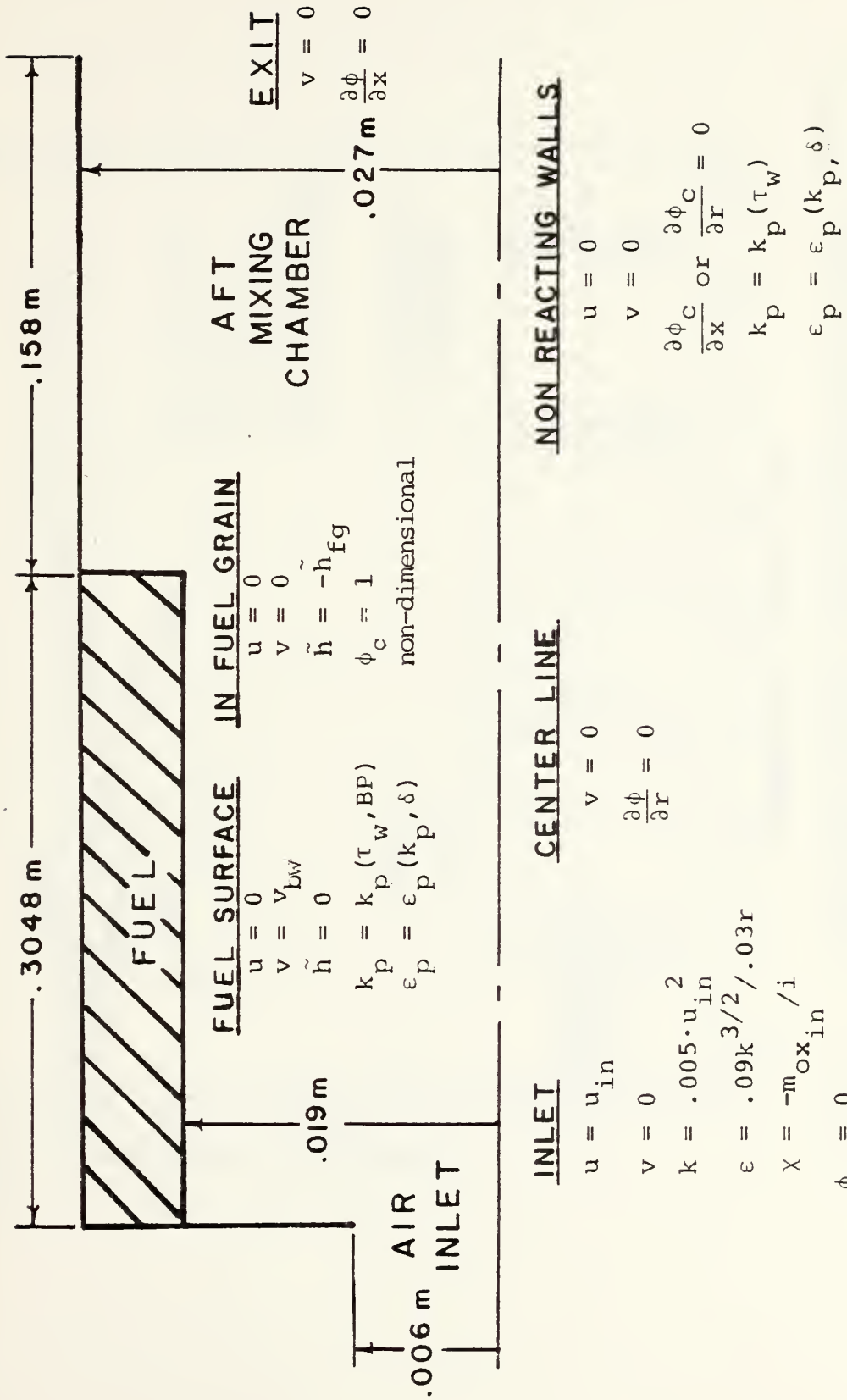
FIGURE 2. SOLID FUEL RAMJET GEOMETRY AND BOUNDARY CONDITIONS
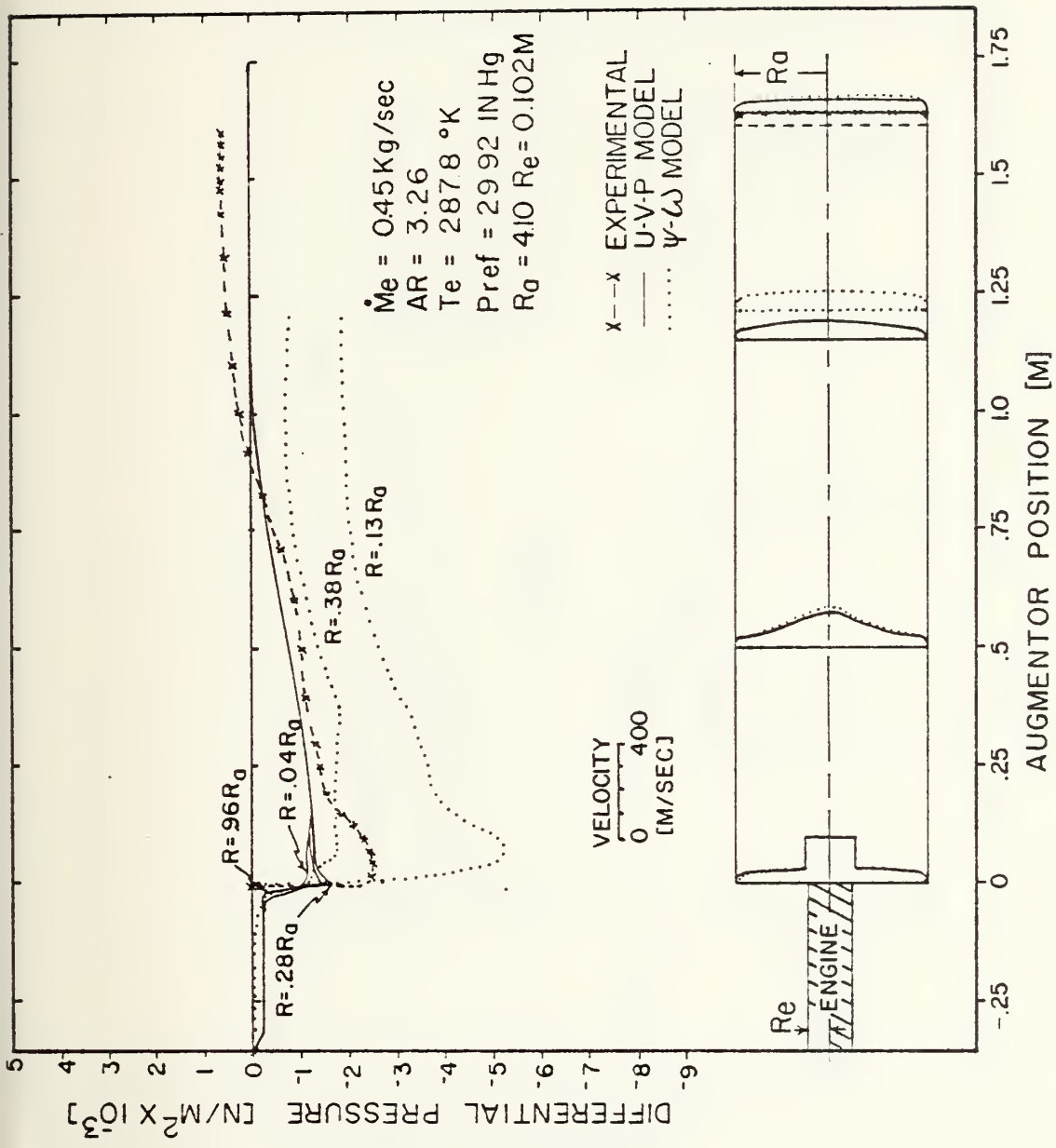
FIGURE 3. AUGMENTOR PRESSURE AND VELOCITY PROFILES FOR STRAIGHT PIPE INLET AND ZERO ENGINE-AUGMENTOR SPACING
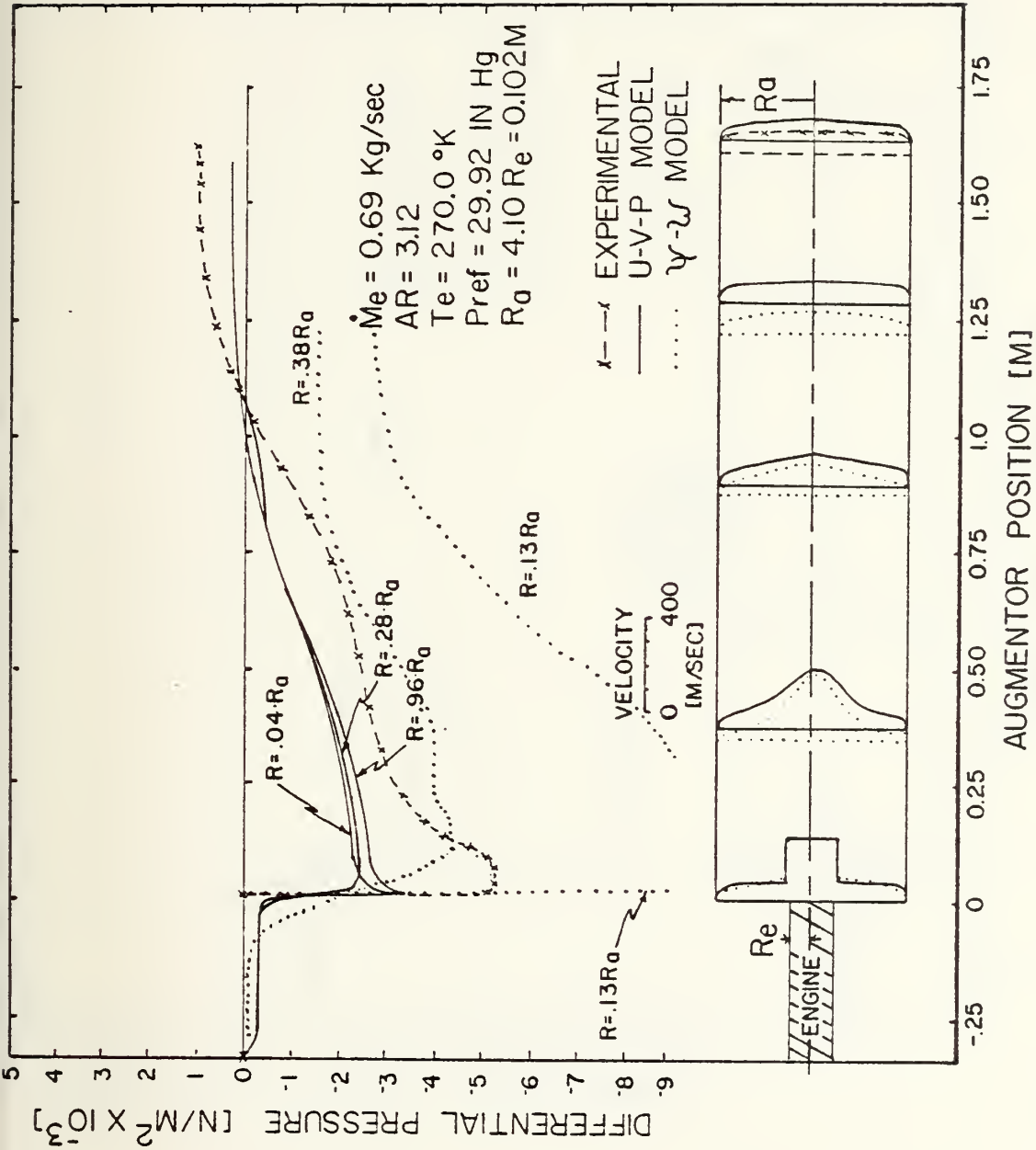
FIGURE 4.   AUGMENTOR PRESSURE AND VELOCITY PROFILES FOR STRAIGHT
PIPE INLET AND ZERO ENGINE–AUGMENTOR SPACING

60
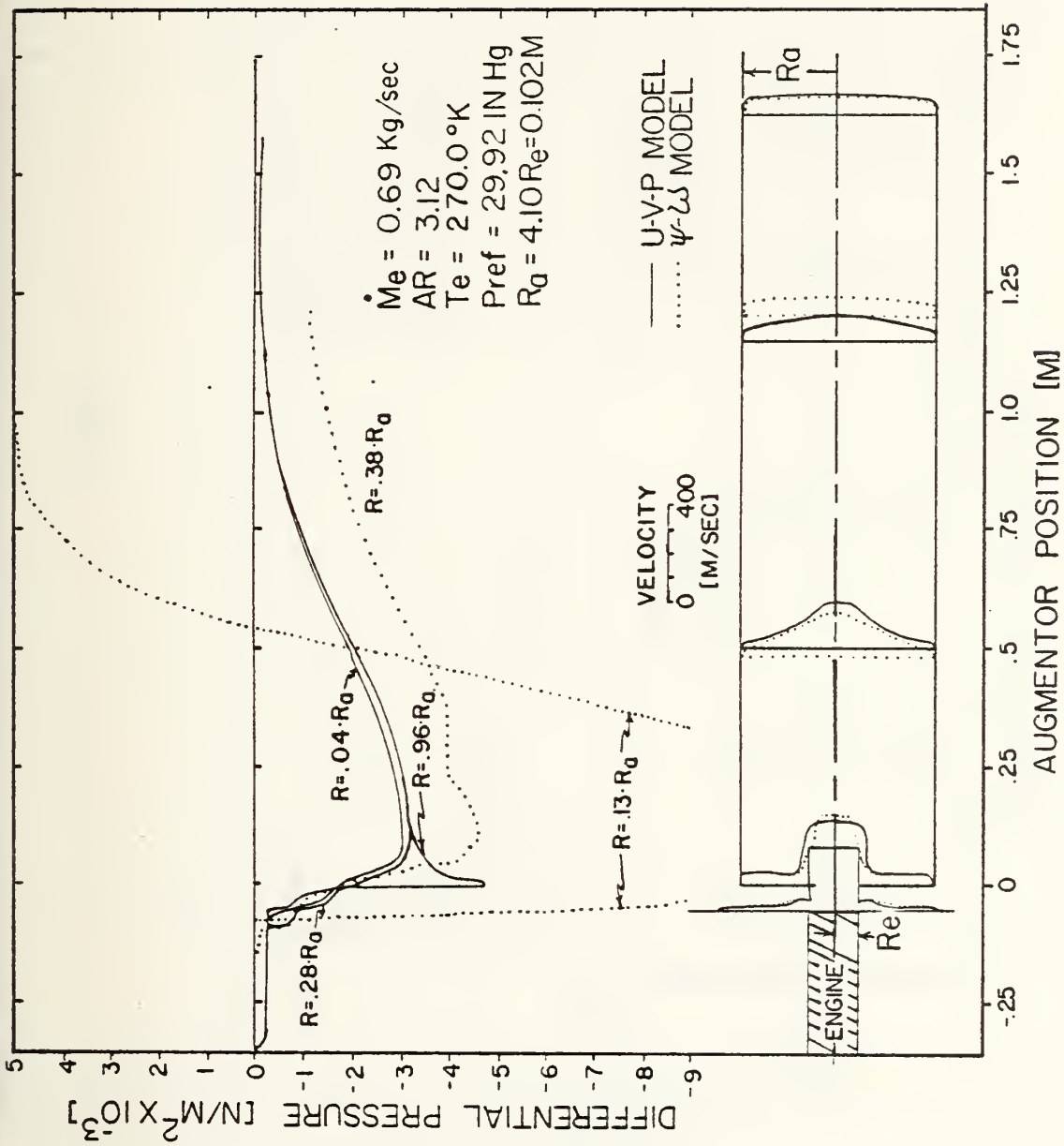
FIGURE 5. AUGMENTOR PRESSURE AND VELOCITY PROFILES FOR STRAIGHT PIPE INLET AND ONE DIAMETER ENGINE-AUGMENTOR SPACING

61
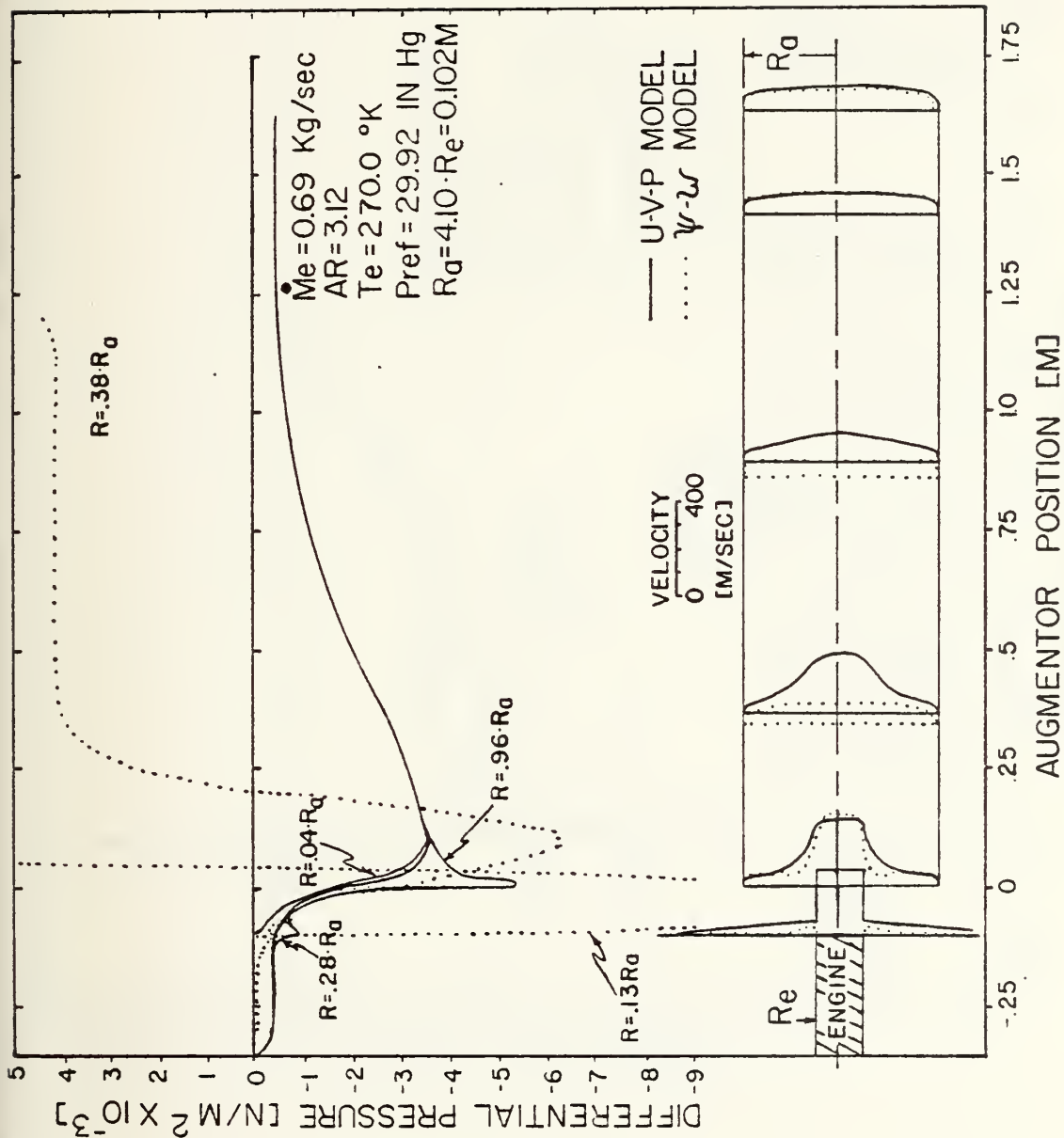
FIGURE 6. AUGMENTOR PRESSURE AND VELOCITY PROFILES FOR STRAIGHT
PIPE INLET AND TWO DIAMETER ENGINE-AUGMENTOR SPACING

62
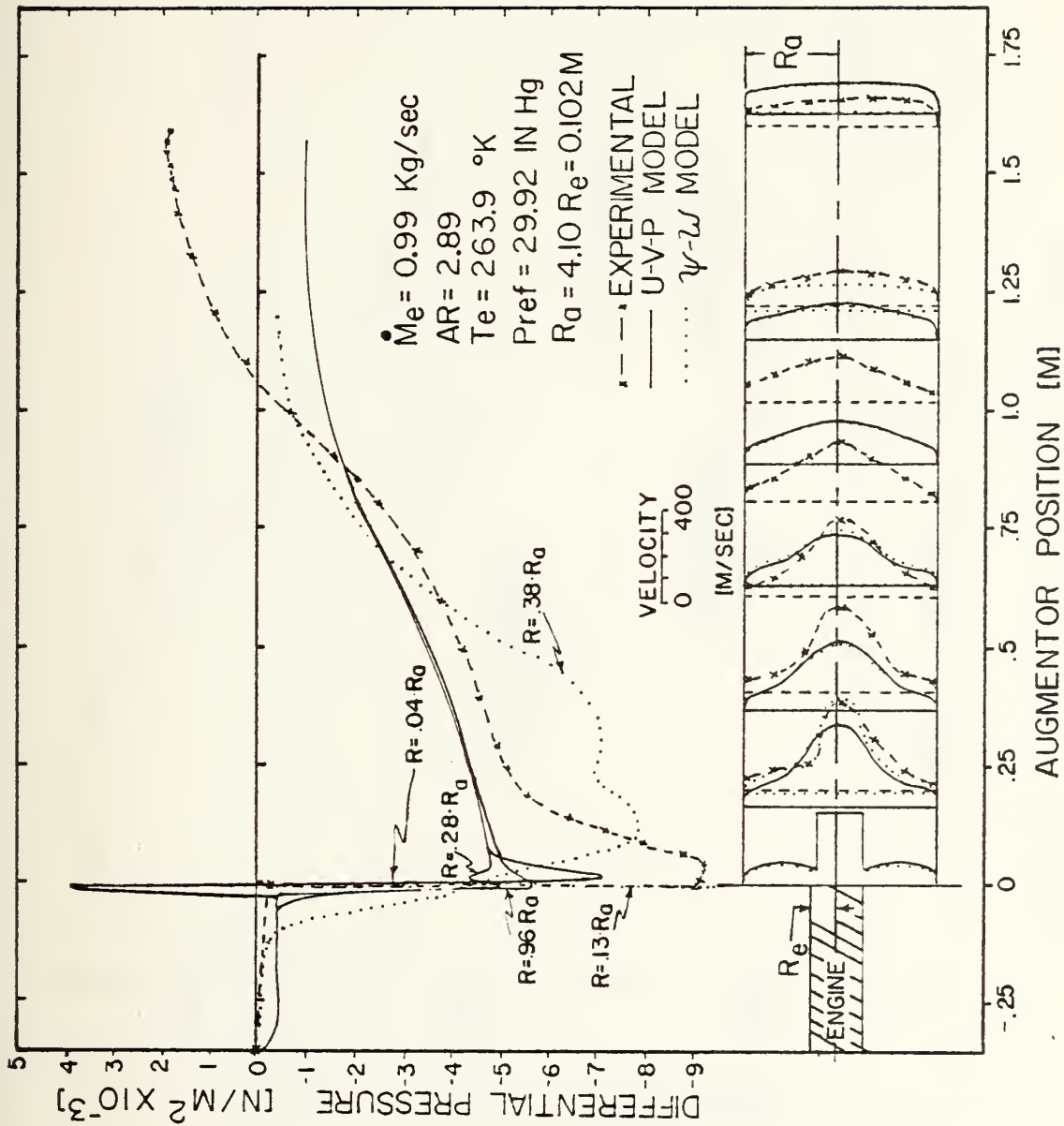
FIGURE 7. AUGMENTOR PRESSURE AND VELOCITY PROFILES FOR STRAIGHT PIPE INLET AND ZERO ENGINE–AUGMENTOR SPACING

63
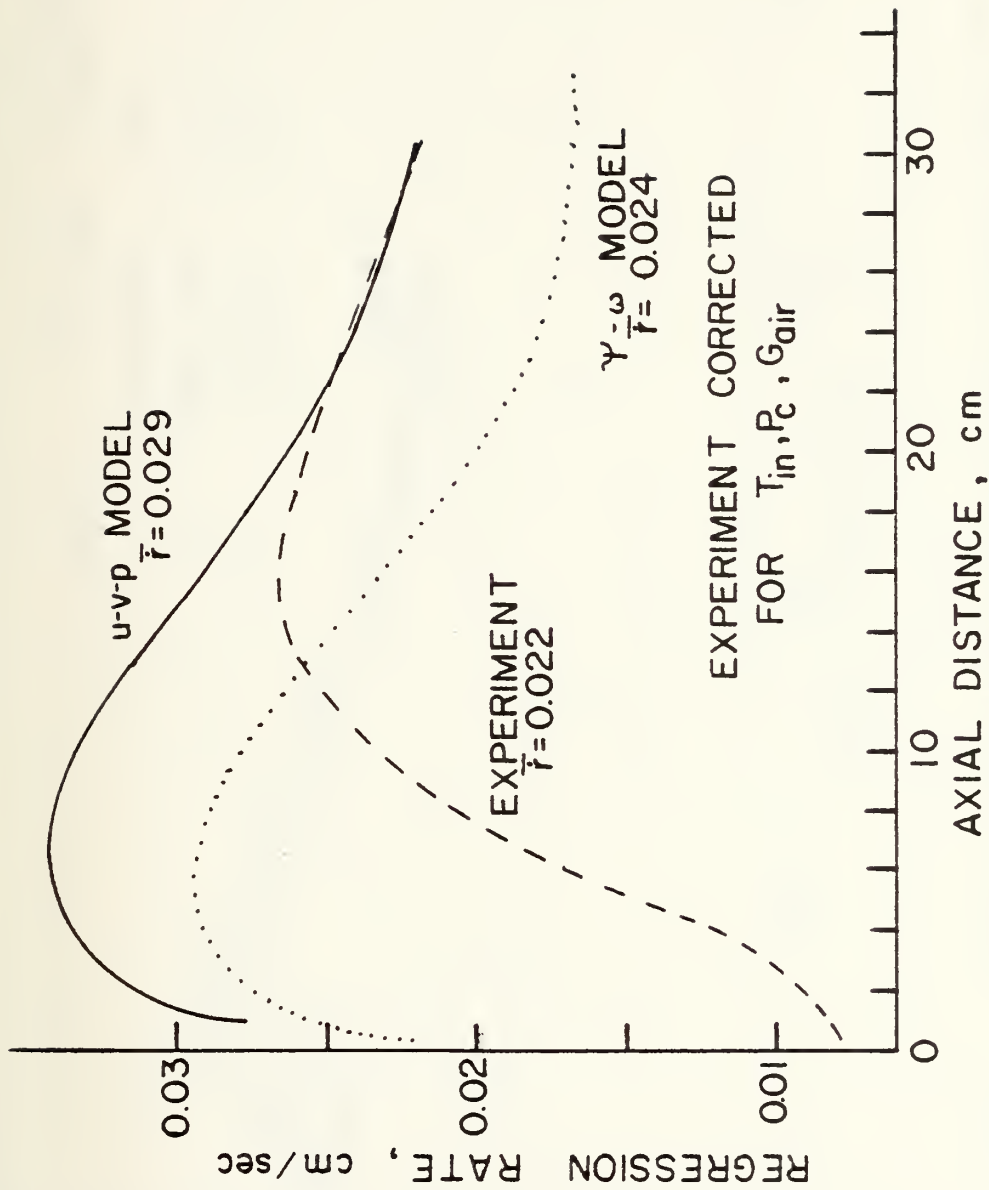
FIGURE 8. PLEXIGLASS REGRESSION RATES
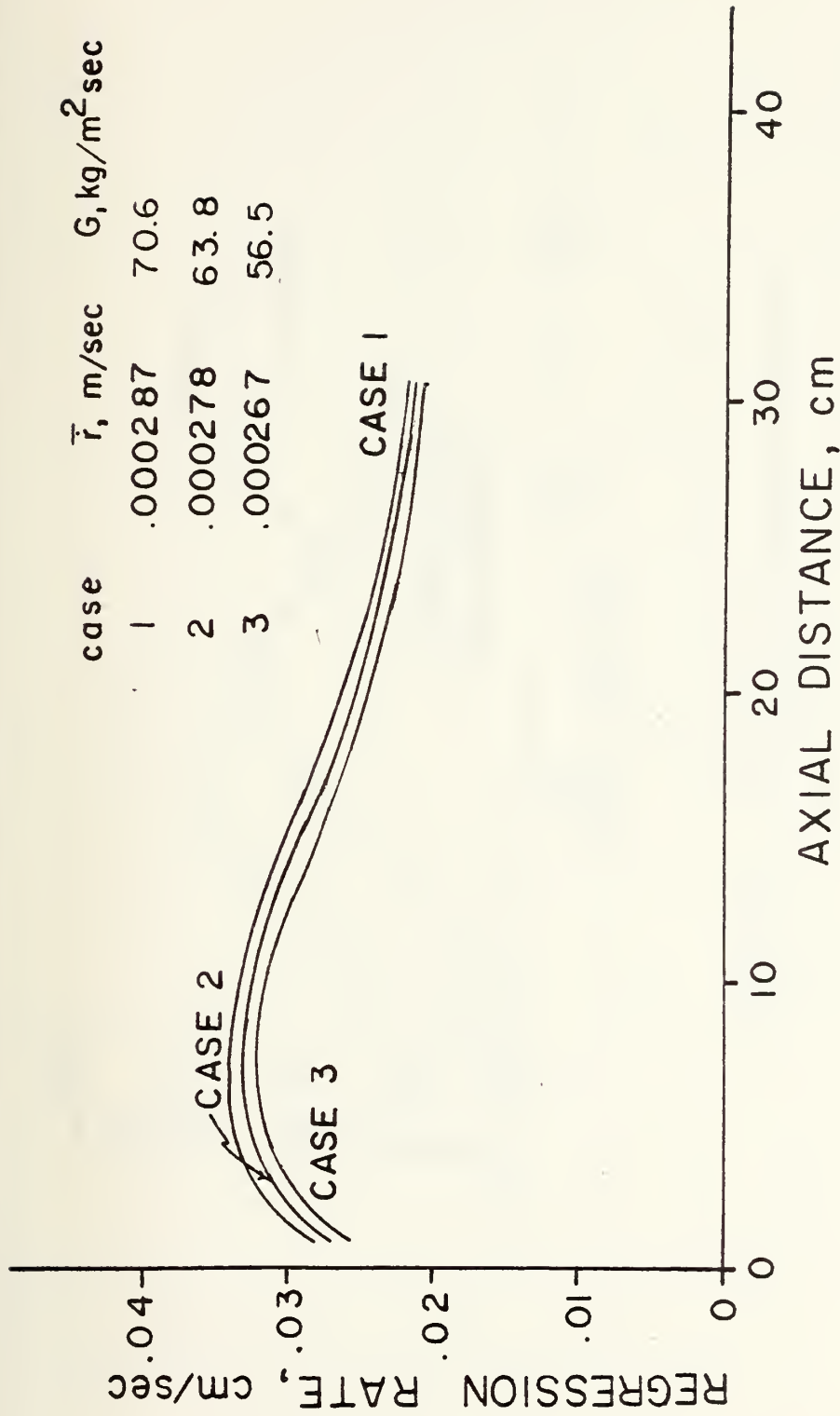
FIGURE 9. EFFECTS OF AIR MASS FLUX ON THE PREDICTED REGRESSION RATES OF THE PRIMITIVE VARIABLE COMPUTER MODEL
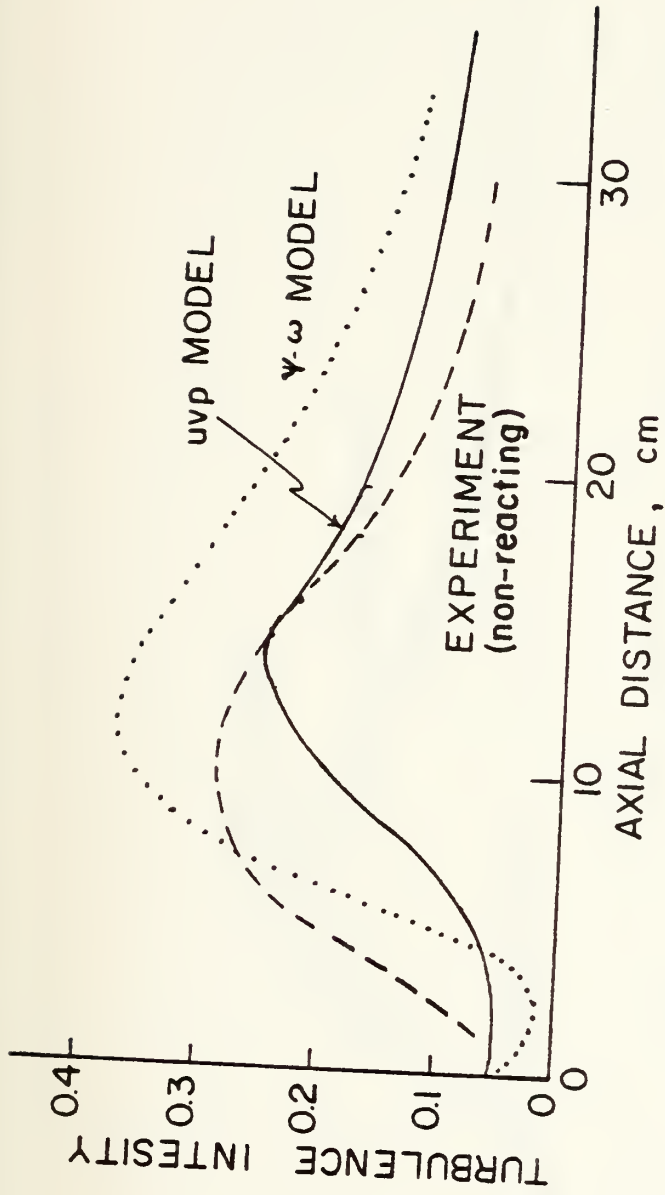
FIGURE 10. CENTERLINE TURBULENCE INTENSITY

$(I \equiv (\frac{2}{3} k)^{1/2} / u)$

66
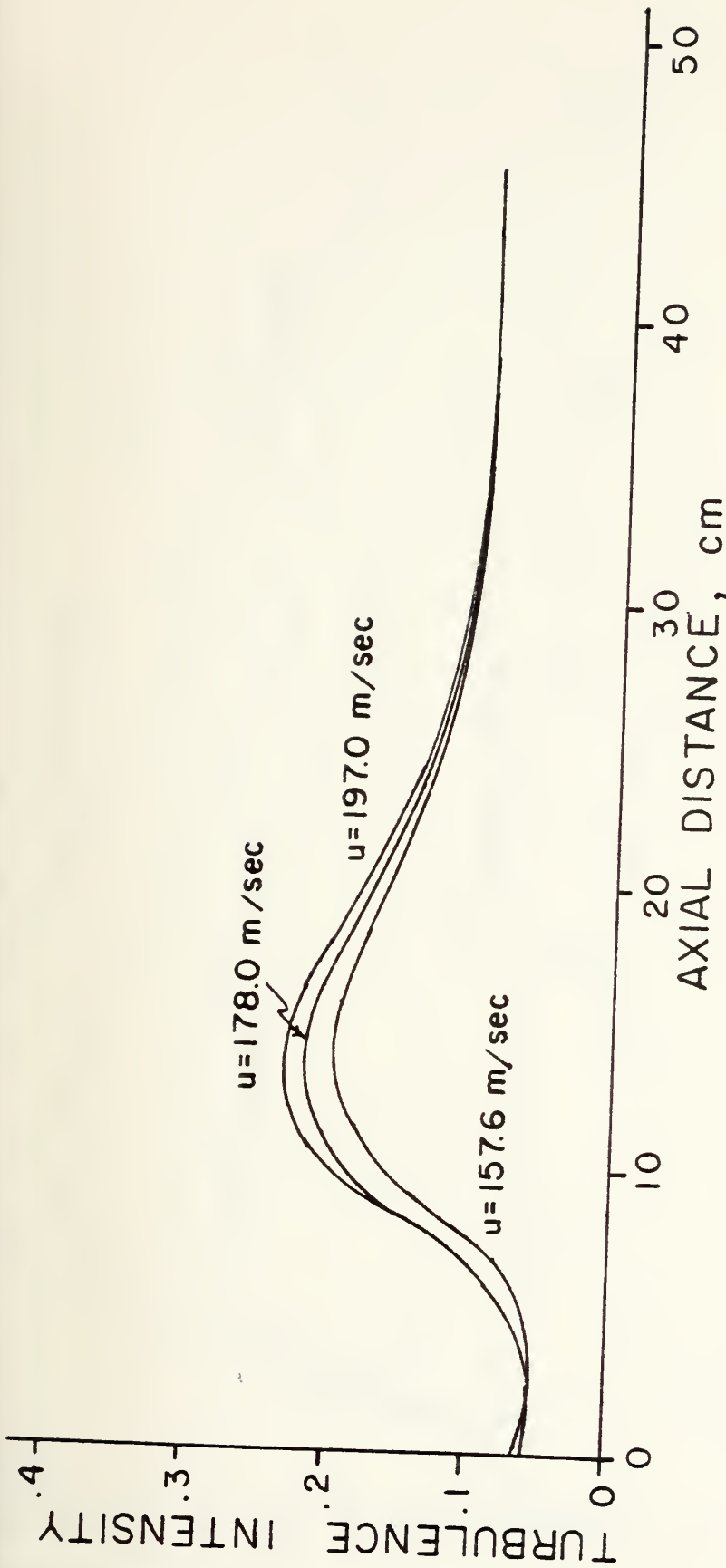
FIGURE 11. PREDICTED CENTERLINE TURBULENCE INTENSITY AS A FUNCTION OF INLET VELOCITY (PRIMITIVE VARIABLE COMPUTER MODEL,

$$I \equiv (\tfrac{2}{3} k)^{1/2} / u)$$

67
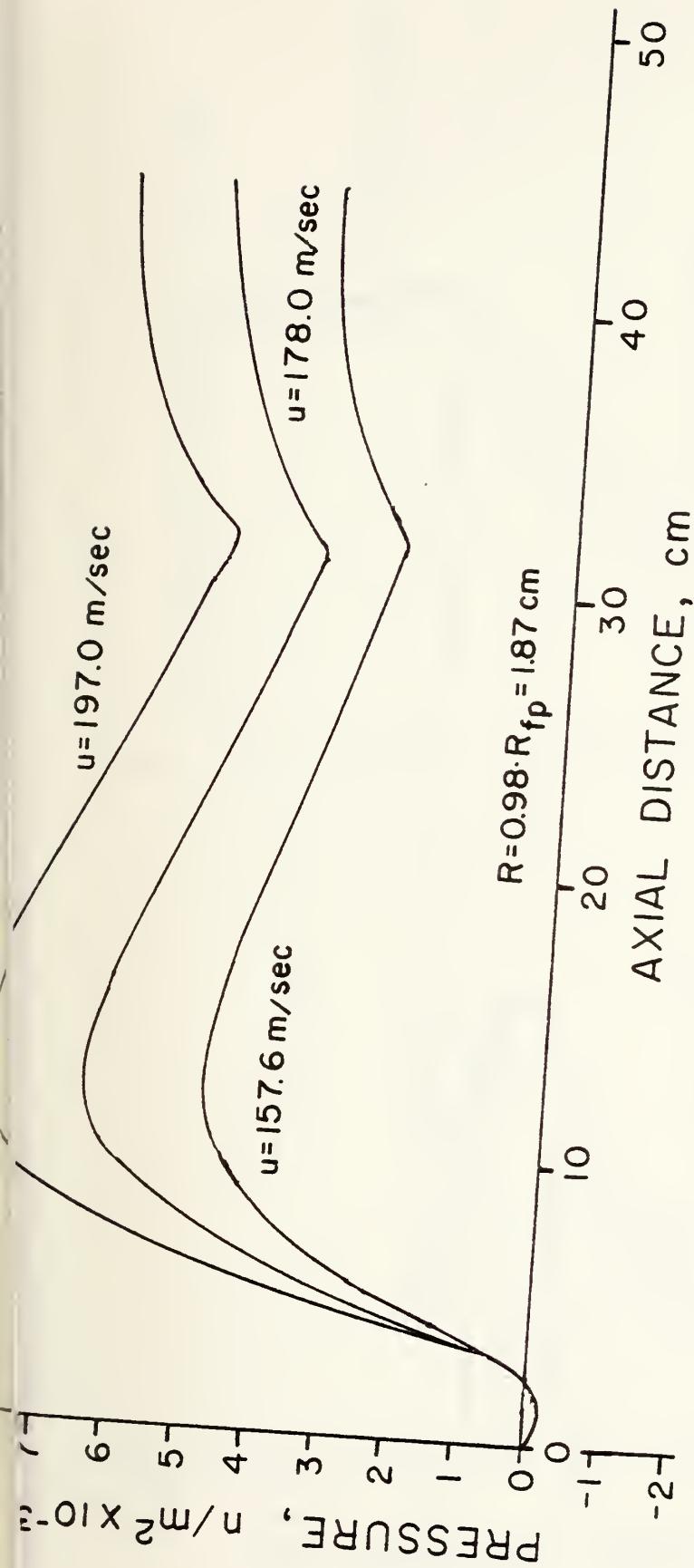
FIGURE 12. PREDICTED AXIAL PRESSURE DISTRIBUTION AS A FUNCTION OF
INLET VELOCITY (PRIMITIVE VARIABLE COMPUTER MODEL)

68
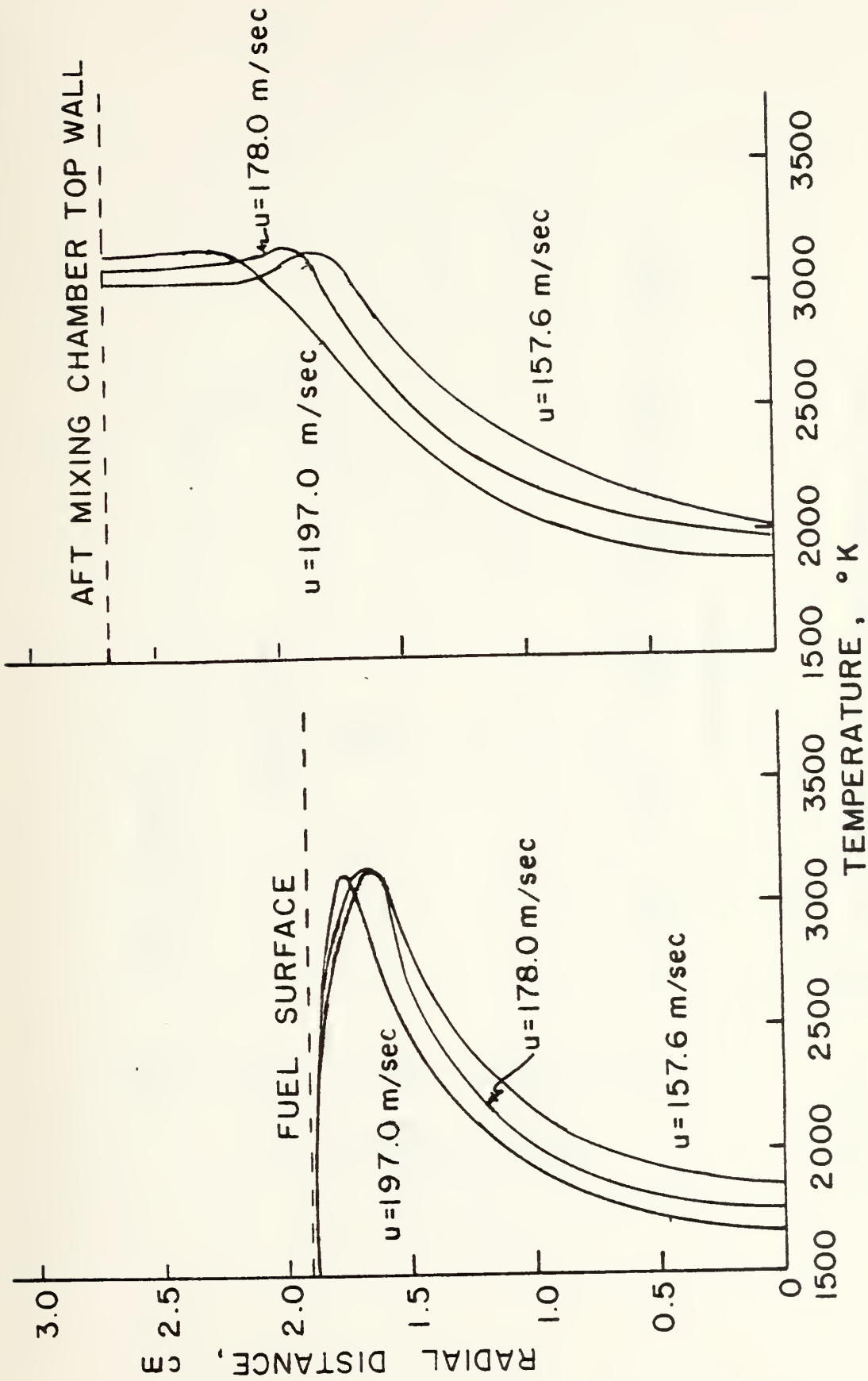
FIGURE 13. PREDICTED COMBUSTOR AND AFT MIXING CHAMBER RADIAL TEMPERATURE
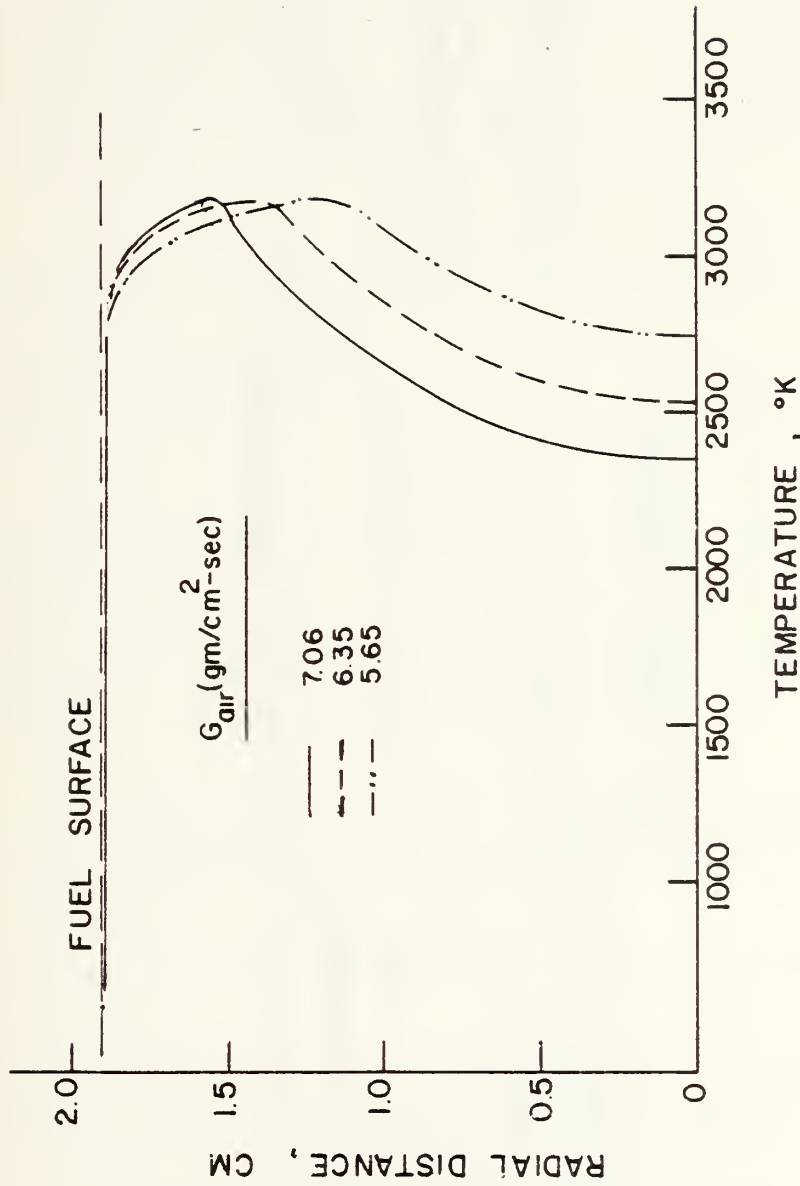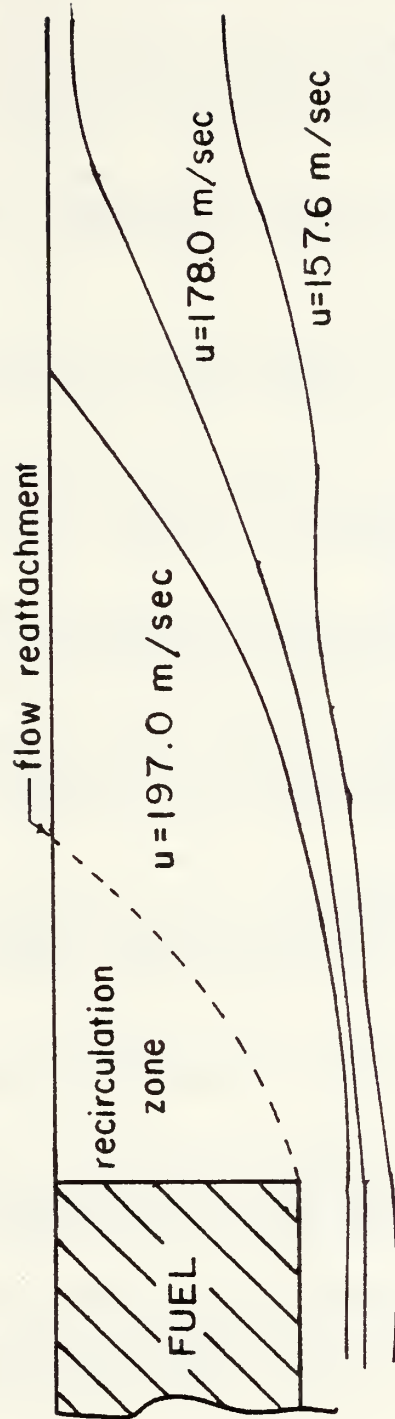VARIATIONS (PRIMITIVE VARIABLE COMPUTER MODEL)

69

FIGURE 14.   PREDICTED RADIAL TEMPERATURE DISTRIBUTIONS
($\psi - \omega$ COMPUTER MODEL, FIGURE 8 OF REFERENCE 5)

FIGURE 15.   PREDICTED FLAME LOCATIONS AND FLOW REATTACHMENT POINT
(PRIMITIVE VARIABLE COMPUTER MODEL)

BIBLIOGRAPHY

1. Gosman, A.D., and others, Heat and Mass Transfer in Recirculating Flows, Academic Press, 1969.

2. Naval Postgraduate School Report Number NPS-57Nt-75101, An Investigation of the Flow in Turbojet Test Cells and Augmenters, by Hayes, J.D. and Netzer, D.W., October 1975.

3. AIRESEARCH Manufacturing Company of Arizona Report Number USARTL-TR-78-55c, Combustor Design Criteria Validation Volume III, by Mongia, H.C. and Reynolds, R.S., February 1979.

4. AIAA Journal, Volume 14, Report Number 10, Finite-Difference Performance Analysis of Jet Pumps, by Croft, D.R. and Lilley, D.G., p. 1347-1378, October 1976.

5. Journal of Spacecraft and Rockets, Volume 14, Report Number 12, Modeling Solid-Fuel Ramjet Combustion, by Netzer, D.W., p. 762-766, December 1977.

6. Naval Postgraduate School Report Number NPS67-78-002, A Validation of Mathematical Models of Turbojet Test Cells, by Walters, J.J. and Netzer, D.W., June 1978.

7. Naval Postgraduate School Report Number NPS-67Nt-76121, Internal Aerodynamics of Turbojet Test Cells, by Speakman, G.C., Hayes, J.D. and Netzer, D.W., December 1976.

8. Pun, W.M. and Spalding, D.B., A General Computer Program for Two-Dimensional Elliptic Flows, Imperical College of Science and Technology, Report No. HTS/76/2, August 1977.

9. Kays, W.M., Convective Heat and Mass Transfer, McGraw-Hill, 1966.

10. Computer Methods in Applied Mechanics and Engineering, The Numerical Computation of Turbulent Flows, by Launder, B.E. and Spalding, D.B., p. 269-289, August 1973.

11. Jones, W.P. and Launder, B.E., "The Predictions of Laminarization with a Two-Equation Model of Turbulence," INT. J. Heat Mass, Transfer, Volume 15, p. 68-87, 1972.

12. Launder, B.E. and Spalding, D.B., <u>Lectures in Mathe-</u>
     <u>matical Models of Turbulence</u>, 2nd ed., Academic Press,
     1976.

13. Naval Postgraduate School Report Number NPS-57Nt73031A,
     <u>An Investigation of the Internal Ballistics of Solid</u>
     <u>Fuel Ramjets</u>, by Boaz, L.D. and Netzer, D.W., March 1973.

14. Naval Postgraduate School Report Number NPS-67Nt77092,
     <u>An Investigation of the Combustion Behavior of Solid</u>
     <u>Fuel Ramjets</u>, by Mady, C.J., Hickey, P.J. and Netzer,
     D.W., September 1977.

INITIAL DISTRIBUTION LIST

No. Copies

1. Defense Documentation Center   2
   Cameron Station
   Alexandria, Virginia 22314

2. Library, Code 0142   2
   Naval Postgraduate School
   Monterey, California 93940

3. Department Chairman, Code 67   1
   Department of Aeronautics
   Naval Postgraduate School
   Monterey, California 93940

4. Professor D. W. Netzer, Code 67Nt   2
   Department of Aeronautics
   Naval Postgraduate School
   Monterey, California 93940

5. Professor R. H. Nunn, Code 69Nn   1
   Department of Mechanical Engineering
   Naval Postgraduate School
   Monterey, California 94940

6. LT C. A. Stevenson, USN   2
   269 "F" Avenue
   Coronado, California 92118